




OPEN Mycosynthesis of zinc oxide nanoparticles using *Mucor racemosus* with their antimicrobial, antibiofilm, anticancer and antioxidant activities

Fathy M. Elkady¹, Bahaa Mohammed Badr^{2,3}, Ebrahim Saied⁴, Amr H. Hashem⁴✉, Mohammed S. Abdulrahman^{1,5}, Mohammad M. Alkherkhis⁶, Tharwat A. Selim⁷ , Fahad M. Alshabrm⁸, Eid A. Alatawi⁹, Faris F. Aba Alkhayl⁸, Ayman Salama¹⁰, Moselhy S. Mansy¹ & Mohammed Aufy¹¹✉

The unregulated administration of currently available antimicrobial agents resulted in overspreading of resistant microbial phenotypes. In this study, *Mucor racemosus* was used for biosynthesis of zinc oxide nanoparticles (ZnO NPs) through fungi-based ecofriendly approach. The biosynthesis of ZnO NPs was initially considered based on analytical practices including UV–vis spectroscopy and transmission electron microscopy (TEM). Additionally, their cytotoxicity and anticancer activity were analyzed using suitable cell lines and their antioxidant effect was also assessed. Microbiologically, their inhibitory activity was comparatively evaluated against various methicillin-resistant *Staphylococcus aureus* (MRSA) and methicillin-sensitive *Staphylococcus aureus* (MSSA). Characterization of ZnO NPs displayed a distinct maximum absorption peak at 320 nm appeared in the UV–vis. Also, TEM revealed predominantly spherical ZnO NPs with particle size distribution ranging from 15 to 55 nm (mean size \approx 40 nm). The normal cell line (Wi-38) illustrated the biosafety of ZnO NPs, where results showed IC_{50} of 197.2 μ g/mL. Furthermore, ZnO NPs exhibited promising suppressive activity on Hep-G2 cancerous cell with IC_{50} of 51.4 μ g/mL. Besides, ZnO NPs displayed antioxidant activity where IC_{50} was 69.2 μ g/mL. As well, the minimum inhibitory concentrations of ecofriendly ZnO NPs against the tested MRSA and MSSA isolates were ranged from 32 to 512 μ g/mL. Also, their minimum bactericidal concentrations against the tested MSSA was in lower range, 32–1024 μ g/mL, than the recorded range, 128–1024 μ g/mL, against the MSSA. Also, the crystal violet (CV) assay showed an eradication potential of the biosynthesized ZnO NPs on MRSA and MSSA biofilm in a range of 23.24–73.96% and 6.63–74.1%, respectively. In conclusion, the ecofriendly synthesized ZnO NPs with antioxidant and anticancer activities demonstrated promising inhibitory effect on planktonic growth form of MRSA and MSSA clinical isolates with capability to eradicate their preformed biofilm. To achieve their full potential, future research needs to enhance the synthesis process to make ZnO NPs more uniform and scalable, as well as investigate their action mechanisms at the molecular level.

Keywords Zinc nanoparticles, Biosynthesis, Fungi, Anticancer activity, Antimicrobial activity, Antioxidant activity

¹Microbiology and Immunology Department, Faculty of Pharmacy (Boys), Al-Azhar University, Cairo, Egypt.

²Department of Basic and Clinical Medical Sciences, Faculty of Dentistry, Zarqa University, Zarqa, Jordan.

³Department of Medical Microbiology and Immunology, Faculty of Medicine, Al-Azhar University, Assiut, Egypt.

⁴Botany and Microbiology Department, Faculty of Science, Al-Azhar University, Cairo 11884, Egypt. ⁵Department of Microbiology and Immunology, Faculty of Pharmacy, Menoufia National University, Menoufia, Egypt.

⁶Department of Microbiology and Immunology, Faculty of Medicine, Al-Azhar University, Cairo 11884, Egypt. ⁷Zoology and Entomology Department, Faculty of Science (Boys), Al-Azhar University, Nasr City, Cairo 11884, Egypt.

⁸Department of Medical Laboratories, College of Applied Medical Sciences, Qassim University, 51452 Buraydah, Saudi Arabia.

⁹Department of Medical Laboratory Technology, Faculty of Applied Medical Sciences, University of Tabuk, 71491 Tabuk, Saudi Arabia. ¹⁰Department of Pharmaceutics, Faculty of Pharmacy, University of Tabuk, 71491 Tabuk,

Tabuk, Saudi Arabia. ¹¹Department of Pharmaceutics, Faculty of Pharmacy, University of Tabuk, 71491 Tabuk, Saudi Arabia.

Saudi Arabia. ¹¹Division of Pharmacology and Toxicology, Department of Pharmaceutical Sciences, University of Vienna, Vienna, Austria. ✉email: amr.hosny86@azhar.edu.eg; mohammed.aufy@univie.ac.at

Staphylococcus aureus (*S. aureus*), a foremost human pathogenic Grampositive bacteria, associated with wide range of slight soft tissue infections and life-threatening chronic disorders¹. The misuse or overuse of antimicrobial agents resulted in spreading of antimicrobial resistant *S. aureus* phenotypes including MRSA in communities and hospitals². The MRSA particular phenotype showed first penicillin resistance in 1948s followed by resistance to methicillin and its related semisynthetic penicillins³. This phenotype is particularly a significant public health threat because it is resistant to over one antimicrobial class, namely beta-lactams including penicillins, cephalosporins, carbapenems, monobactams, cepheids, and β -lactams/ β -lactamase inhibitors, which dramatically lowers the number of drugs available for treatment⁴. Also, MRSA bacterial phenotype pose significant health threats to the global world as they can cause serious superficial skin and soft tissue infections, pneumonia, sepsis, and endocarditis⁵. Furthermore, human illness associated with MRSA strains have difficult and restricted treatment options due to spreading of multi-drug resistant (MDR) MRSA strains and mostly resulted in high mortality rate⁶. On the other hand, MSSA, being methicillin-susceptible but challenging to deal with due to virulence factors and the hazard of rapid infection progression, demands effective mitigation tools in both healthcare and community settings⁷. The bacterial cells adhesion, aggregation, biofilm structure maturation, and spreading represent the stages of the readily developed *S. aureus* biofilm with enhanced antimicrobial-resistance⁸. Consequently, *S. aureus* strains biofilms has a considerable impact on host immune responses against this pathogen⁹. Therefore, there arises a pressing demand for innovative methods of mitigation. Some recent advancements against such infections include the identification of novel antimicrobial agents such as lipoglycopeptides and bacteriophage therapy¹⁰. Despite all these advancements, MRSA and MSSA are still a challenge due to evolving resistance mechanisms, biofilm formation, and no excellent vaccine. The global burden is also fueled by inefficient surveillance mechanisms, inappropriate antimicrobial use, and unavailable advanced diagnostics in resource-constrained settings, making containment of such pathogens a perennial challenge¹¹.

The unveiling of unusual and suitable alternates to control such infectious pathogens has become a highly endorsed target to control the continuous emergency of MDR pathogenic phenotype as well as, to overcome the time-consuming, labor-intensive, and expensive methods for new antimicrobial assembly¹². The nano structure-based antimicrobials could become an excellent paradigm to combat infectious agents with various antimicrobial resistant behavior^{13,14}. The nanoparticles (NPs) toxicity may be resulted from their tiny size which facilitates their biological barriers penetration with strong interaction and efficient targeting of microbial cells¹⁵. Nanoparticles have garnered significant attention from researchers across various scientific fields^{16–18}. These particles were generally categorized as inorganic and organic NPs¹⁹. The inorganic group includes metallic, semi-metallic, and magnetic NPs, whereas the organic group primarily consists of carbon-based NPs²⁰. The application of typical nano-scaled materials, with size range from 1 to 100 nm, represents a rapidly advancing field within nanoscience and nanotechnology²¹. In essence, nanotechnology involves manipulating materials at the atomic scale through a combination of engineering, chemical, and biological techniques. As a contemporary concept, nanotechnology has become amongst major and extensively studied parts of advanced science^{22,23}.

Zinc (Zn) is a transition metal with excellent electrical and thermal conductivity, widely recognized for its essential role in biological systems²⁴. Zinc oxide nanoparticles exhibit unique physicochemical properties, including a wide bandgap (~3.37 eV), high surface area, and remarkable stability, making them suitable for various biomedical applications²⁵. Additionally, ZnO NPs demonstrate significant reactive oxygen species (ROS) generation, which contributes to their antimicrobial and oxidative stress-modulating properties²⁶. Their inherent biocompatibility and low toxicity further support their potential for safe and controlled applications^{27,28}.

ZnO NPs were selected for this study due to their well-documented antimicrobial efficacy, selective cytotoxicity, and strong antioxidant activity. Their stability, biocompatibility, and environmentally friendly synthesis make them promising candidates for biomedical and pharmaceutical applications, aligning with the principles of green nanotechnology^{29,30}.

ZnO NPs synthesis can be achieved through two primary approaches, bottom-up and the top-down techniques³¹. In bottom-up approach, the structures constructed via atom by atom or molecule by molecule relying on self-assembly. Conversely, the top-down method reduces the size of a bulk material into nanoscale dimensions using physical or chemical techniques. Both approaches are commonly employed for NPs production^{32,33}. Synthesis of NPs following chemical or physical technique usually employ harsh conditions, such as exposure to toxic chemicals, elevated pressures, and high temperatures. These factors can have environmental impacts or demand the use of advanced equipment³⁴. On the other hand, the biological approach, also known as green technology, offers an environmentally friendly alternative utilized in NPs preparation. Nanotechnology integration with biological sciences provided new avenues for various scientific fields research³⁵. Biological systems have been suggested as environmentally friendly alternatives to traditional physicochemical methods³⁶. These systems utilize bacteria, fungi, algae or extracts from various plants as a source of capping agents to stabilize NPs^{37–44}. Fungi are particularly well-suited in biogenic ZnO NPs synthesis due to their remarkable metal tolerance with ease of cultivation. In addition, they produce substantial amounts of extracellular proteins that are essential for NPs stabilization⁴⁵. Compared to bacterial systems, fungal cultures offer several benefits, including greater biomass yield and the elimination of extra extraction procedures⁴⁶. *Mucor racemosus*, a filamentous fungus, was chosen for ZnO NP synthesis due to its strong biogenic potential and enzymatic activity. This fungus secretes various extracellular metabolites, such as proteins, polysaccharides, and organic acids, which aid in metal ion reduction and nanoparticle stabilization^{47,48}. These biomolecules naturally cap the nanoparticles, enhancing their stability, minimizing aggregation, and influencing their morphology⁴⁹. Furthermore, fungal-derived functional groups can modify the surface properties of ZnO NPs, potentially improving their biocompatibility

and antimicrobial effectiveness²⁷. The interaction between *Mucor racemosus* and ZnO NPs may also regulate nucleation and growth, leading to well-defined nanoparticles with favourable physicochemical traits. This green synthesis approach presents a safer and more sustainable alternative to conventional chemical methods, minimizing toxicity and environmental impact⁵⁰.

Also, fungi demonstrated significant capability in large-scale NPs synthesis⁵¹. Additionally, the adaptability of ZnO NPs associated with their wide utilization as antibacterial agents as well as other areas including medicinal diagnosis, electronics, and catalysis^{27,52,53}. Additionally, they exhibit promising properties like anticoagulant, antidiabetic, and thrombolytic activities. Although, the common utilization of physical and chemical methods to synthesize ZnO NPs, such approaches are often expensive and pose environmental concerns⁵⁰. Recently, the biosynthesis of ZnO NPs has progressed rapidly, offering an ecological, cleaner, non-hazardous, and biosafe alternative for conventionally utilized physical or chemical techniques^{50,54}. In comparing with other metal oxide NPs, ZnO NPs possess wide arrangement of medical applications, including drug delivery, imaging, cancer treatments, anti-inflammatory effects, antibacterial and antidiabetic therapies, and wound closing^{55,56}.

While ZnO NPs have attracted considerable attention for biomedical applications, their large-scale, eco-friendly synthesis using fungal-mediated approaches remains insufficiently explored. This study presents an innovative mycosynthetic method for ZnO NPs using *Mucor racemosus*, providing a more sustainable and cost-effective alternative to conventional chemical and physical techniques. The extracellular proteins produced by *Mucor racemosus* contribute to nanoparticle stability, aligning with green nanotechnology principles and minimizing the environmental impact associated with chemical synthesis.

The core hypothesis of this research is that fungal-derived ZnO NPs will exhibit; (a) notable cytotoxicity against Hep-G2 cancer cells while preserving biocompatibility with normal human fibroblast cells (Wi-38). (b) Superior antimicrobial properties, particularly against biofilm-forming MRSA and MSSA clinical isolates, positioning them as a potential alternative for managing multidrug-resistant infections. (c) Strong antioxidant activity, highlighting their prospective role in mitigating oxidative stress-related disorders. The stability of the synthesized ZnO NPs in physiological conditions, including their behavior in biological fluids, has been addressed in the discussion section. This addition provides insights into factors influencing their stability, such as biomolecular capping, zeta potential, and dissolution behavior, which are crucial for their potential biomedical applications⁵⁷. This study not only investigates the biological activity and therapeutic potential of ZnO NPs but also addresses key challenges related to their stability, selective cytotoxicity, and antimicrobial mechanisms. Through a biogenic synthesis approach, the research aims to advance the development of safe, scalable, and multifunctional nanomaterials for future biomedical applications. The study aimed to biosynthesize eco-friendly zinc oxide nanoparticles (ZnO NPs) using *Mucor racemosus* to combat antimicrobial resistance. The ZnO NPs were characterized using UV–vis spectroscopy and TEM, and their cytotoxicity, anticancer, antioxidant, and antimicrobial activities were evaluated against MRSA and MSSA, including biofilm disruption.

Materials and methods

Chemical and reagents

Analytical grade Zinc nitrate hexahydrate ($\text{Zn}(\text{NO}_3)_2 \cdot 6\text{H}_2\text{O}$), sodium hydroxide (NaOH) of 99% purity, and malt extract agar (MEA) and malt extract broth (MEB) fungal growth media utilized in the current work were bought from Sigma Aldrich in Cairo, Egypt. In all biological experiment, distilled water (dH_2O) was utilized.

Clinical specimens and bacterial isolates

The examined 42 *S. aureus* clinical isolates were supplied by Microbiology Lab., Sayed Galal Teaching hospital, Al-Azhar University, Cairo, Egypt. These isolates were phenotypically identified and initially confirmed according to the Procop et al.⁵⁸ guidelines. In brief, culture characteristics on nutrient agar, mannitol salt agar (MSA), and blood agar plates were considered for primary isolate identification. Light microscope examination of Gram-stained smears was then applied for detection of Gram reaction type and bacterial cells morphology and arrangement. As well, biochemical assays for catalase, coagulase, oxidase, and DNase tests were conducted for basic phenotypic identification of *S. aureus* isolates¹³.

Phenotypic and genotypic confirmation of MRSA

Firstly, the initial phenotypic differentiation between MRSA and MSSA isolates were conducted via oxacillin resistance screen agar test which assess the ability of the tested *S. aureus* isolates for growing on MSA supplemented with oxacillin resistance screening agar base (ORSAB) (Oxoid LTD, Basingstoke, UK)⁵⁹.

As a confirmatory test, all the tested *S. aureus* isolates were secondly characterized following the cefoxitin disc diffusion test⁶⁰. In brief, each tested bacterial suspension, adjusted to 0.5 McFarland, aseptically cultured into Muller Hinton agar (MHA) plate (Oxoid, UK) to obtain lawn bacterial growth followed by quietly placing of cefoxitin disc (30 µg) (Oxoid, UK). Following the incubation for 18 h at 35 °C, the inhibition zone diameter (IZD) around the tested disc was measured.

After confirmed identification of the tested isolates as phenotypically MRSA or MSSA, they were genotypically confirmed via PCR detection of the resistance-associated *mecA* virulence determinant⁶¹. In brief, the PCR amplification mixture was of genomic DNA extracted by boiling method (1 µL), *mecA* gene specific forward 3'-GTGAAGATATACCAAGTGATT-5' and reverse 3'-ATGCGCTATAGATTGAAAGGAT-5' primers (1 µL) each, Cosmo PCR Red Master Mix (Willowfort, UK) (12.5 µL), and nuclease-free water (9.5 µL). Negative control containing all reaction mixture without bacterial DNA was included. The amplification program started with an initial denaturation phase at 94 °C for 4 min for 1 cycle followed by elongation phase of 35 cycles of: denaturation at 94 °C for 60 s, annealing at 55 °C for 60 s, and elongation at 72 °C for 60 s, and the amplification program completed with a final elongation phase for 10 min at 72 °C.

Ethidium bromide stained agarose gel (1.5%) was employed for separation of the obtained PCR products based on electrophoresis at 100 V using Tris-acetate EDTA buffer (Sigma Aldrich, Germany) for 45 min. The stained *mecA* gene-specific bands was observe by UV transilluminator (HERMLE Labortechnik GmbH, Germany) and their molecular size determine by comparing with the 100 bp DNA ladder (Geneaid Biotech Lt., Taiwan).

Fungal growth conditions

Mucor racemosus (accession number MG547571) was isolated during our previous research⁶². *Mucor racemosus* was inoculated onto MEA and incubated at 30 ± 2 °C for 7 days, the fungus was preserved until use at 4 °C^{63,64}.

Mucor racemosus mediated ZnO NPs

In 100 mL MEB, 2 *Mucor racemosus* disks were inoculated followed by incubation with shaking (200 rpm) for 7 days at 30 ± 2 °C. The fungal biomass was then collected by centrifugation and resuspended in 100 mL dH₂O for 48 h at 30 ± 2 °C with shaking at 200 rpm followed by filtration using Whatman filter paper (No.1). Zinc nitrate (4 mM) was then added to the filtrate, incubated for 12 h with shaking (200 rpm) at 32 °C, with pH adjustment to 8. The negative control experiment was included using dH₂O instead of the tested fungal extract. The reduction process was considered based on the production of white precipitate that was collected by centrifugation for 7 min at 15,000 rpm, rinsed using dH₂O to eliminate all persisting contaminants, and oven-dried at 200 °C for 6 h⁶⁵.

Characterization of ZnO NPs

The establishment of ZnO NPs were fully characterized depending on various analysis. The created ZnO NPs using cell-free *Mucor racemosus* filtrate was analyzed and confirmed using UV-vis spectrophotometer (JENWAY 6305 spectrophotometer) to measure absorbance between 300 and 800 nm. Additionally, the X-ray diffraction (XRD) profile was documented using Cu-K α radiation where the values of 2θ was measured between 4° and 80° through X'Pert Pro diffractometer (Philips, Eindhoven, Netherlands). The Debye-Scherrer equation was utilized for calculation of ZnO NPs average size⁶⁶. Dynamic light scattering (DLS) (Malvern Instruments Ltd. in Worcestershire called the Malvern Zetasizer Nanoseries) was conducted for estimation of size distribution of different dispersed ZnO NPs. The biosynthesized NPs morphology was determined based on TEM imaging (JEM1230, Japan, Akishima, Tokyo, 196–8558). The Fourier transform infrared (FTIR) spectra of ZnO NPs was studied at 400–4000 cm⁻¹ (Agilent System Cary 660 FT-IR Model).

Antioxidant activity

In the current study, different ZnO NPs and ascorbic acid (standard control) concentrations in the range of 3.12–200 µg/mL were examined for their diphenyl picrylhydrazyl (DPPH) radicals scavenging ability. The DPPH solution (800 µL) was mixed with each tested concentration (200 µL) with profuse shaking, and kept in darkness for 30 min at 25 °C followed by centrifugation at 13,000 rpm for 5 min⁶⁷. Each tested concentration absorbance was measured at 517 nm in comparison with a blank. Antioxidant activity percentage was calculated by the following Equation:

$$\text{Antioxidant activity (\%)} = \frac{\text{Control absorbance} - \text{Sample absorbance}}{\text{Control absorbance}} \times 100$$

In vitro cytotoxicity and anticancer activity

The biosynthesized ZnO NPs toxicity was determined against Wi-38 normal and Hep-G2 cancerous cell lines using the 3-(4,5-dimethylthiazol-2-yl)-2,5 diphenyl tetrazolium bromide (MTT) protocol⁶⁸ with minor modification. The cell quantity and the percentage of viable cell were totaled by the following Formula, respectively:

$$\text{Viability \%} = \frac{\text{ZnO NPs OD}}{\text{Control OD}} \times 100$$

$$\text{Inhibition \%} = 100 - \text{Viability \%}$$

Microbiological assays

Well diffusion assay

The IZD, that reflect the biosynthesized ZnO NPs initial activity towards MRSA and MSSA, was measured following the agar well diffusion assay conducted under restricted aseptic conditions. In brief, each prepared bacterial isolate suspension of 0.5 McFarland standard concentration inoculated into MHA plate using sterile cotton swab that consent for growth in a lawn form. Four wells were then made on the MHA surface using sterile borer. One hundred microliters from 1000 µg/mL ZnO NPs suspension in dimethyl sulfoxide (DMSO) or 50 µg/mL vancomycin (standard positive control) were then separately inoculated into two wells. The DMSO (8%) and zinc acetate (1000 µg/mL) were inoculated into the remaining two wells as negative controls. Each tested plate was then pre-incubated in the refrigerator for half an hour then incubated at 37 °C for 24 h followed by measuring of the observed IZD around each inoculated well⁶⁹.

Consequently, the percentage inhibition (PI) described by Elkady et al.⁷⁰ of ZnO NPs for all tested isolates was then calculated according to the following Formula:

$$\text{Percent Inhibition (PI)} = \frac{\text{IZD caused by the ZnO NPs}}{\text{IZD caused by vancomycin}} \times 100$$

Broth microdilution assay

The quantitative capability of ZnO NPs to cease the growth of the tested MRSA and MSSA isolates was evaluated following broth microdilution assay. A 96-well microtiter plate was used for determination of each tested bacterial isolate MIC and MBC⁷¹. In brief, the tested ZnO NPs was dissolved in DMSO and two-fold serial dilution, in the range of 512–16 µg/ml, was aseptically constructed in each raw of the microtiter plate using Muller Hinton broth. An equal volume of each tested bacterial suspension (10 µL), at a concentration equivalent to 0.5 McFarland standard, was then added to the wells of each raw with 200 µL final volume. After plates incubation at 37 °C for 24 h aerobically, the prepared resazurin solution (0.015%: 40 µL) was added to each well with additional plates incubation at 37 °C for 2 h. The lowest concentration in each raw without visible blue resazurin color switch into red was recorded as the MIC of ZnO NPs. For each tested isolate, the suspension from all wells with blue color was consequently inoculated into MHA plate followed by incubation for at 37 °C 24 h. The lowest concentration of ZnO NPs caused no visible growth was reported as their MBC. Each tested bacterial strain tolerance to the tested ZnO NPs was then calculated according to the Formula:

$$\text{Tolerance level} = \frac{\text{MBC}}{\text{MIC}}$$

Consequently, the results recorded as NPs bacteriostatic or bactericidal activity at tolerance value ≥ 4 or ≤ 2 , respectively.

Biofilm destructive assay

The CV staining assay, conducted as triplicate using 96 well microtiter plate, was used to evaluate the different capabilities of the tested MRSA and MSSA for biofilm formation and ZnO NPs effect on their preformed bacterial biofilm. Each 0.5 McFarland standard bacterial suspension (10 µL) was inoculated into each well of sterile 96-well microtiter plate containing tryptic soya broth (TSB) containing 1% glucose (TSBG) with a final volume of 200 µL and statically incubated at 37°C for 48 h to allow bacterial cell surface attachment. Afterward, the planktonic bacterial growth was discarded followed by washing of remaining biofilms using phosphate buffered saline (PBS: pH 7.2) three times. Subsequently, two separate test procedure groups were applied.

In the first group, the quantitative ability of MRSA and MSSA isolates for biofilm formation was evaluated in presence of uninoculated TSBG as negative control (NC)⁷². Concisely, after desiccation for 1 h at 60 °C, the bacterial biofilms behind were stained using 2% CV for 15 min followed by discarding of the excess stain and washing with PBS (pH 7.2) three times. The bound dye, in each well, was then dissolved using 33% (v/v) glacial acetic acid (180 µL). Each assay was conducted in triplicate and the optical density (OD) was determined at 570 nm (OD_{570}). Afterwards, the mean OD and standard deviation (SD) for the NC were calculated. Subsequently, the cut-off optical density (OD_c) was determined using the Formula:

$$\text{OD}_c = \text{mean OD of NC} + 3 \text{ SD of NC}$$

The MRSA and MSSA isolates were recorded as; non-biofilm forming at mean OD (OD_m) $\leq \text{OD}_c$, weak-biofilm forming (+) at $\text{OD}_c < \text{OD}_m \leq 2 \text{ OD}_c$, moderate-biofilm forming (++) when $2 \text{ OD}_c < \text{OD}_m \leq 3 \text{ OD}_c$, or strong-biofilm forming (+++) at $3 \text{ OD}_c \geq \text{OD}_m$.

In the second group, the eradication activity of biogenic ZnO NPs against MRSA and MSSA preformed biofilm was assessed⁷³. Concisely, the preformed bacterial biofilm cultivated in presence of the MIC of the tested ZnO NPs at 37°C for another 24 h followed by removing of excess culture media and washing. The CV (1%: 150 µL) solution was added followed by incubation for 15 min. The redundant dye was then rinsed away with PBS (pH 7.2) followed by naturally drying. Finally, the residual biofilms were destained for 20 min using 33% acetic acid and quantified using a microplate reader via determination of OD at 595 nm. The biofilms clearance percentage for each tested material was then calculated following the Formula:

$$\text{Biofilm clearance (\%)} = 1 - \frac{\text{OD}_{595} \text{ of tested material treated cells}}{\text{OD}_{595} \text{ of untreated cells}} \times 100$$

Statistical analysis

The Microsoft Excel 2021 software was used to calculate the mean (M), median, standard deviation (SD), standard error (SE), and relative standard deviation (RSD) from the primary data with consequent presentation of the findings obtained from experiments conducted in triplicates as the mean \pm SD. Furthermore, the correlation coefficient between variables was conducted using Pearson correlation coefficient (r) value by Microsoft Excel 2021, in which a positive value indicate a direct relationship and negative value indicates an inverse relationship. Also, the calculated percentage and frequency descriptive statistics were applied for results investigation. As well, statistical analysis of data including figures construction were managed using the GraphPad Prism v8. Where applicable, one-way analysis of variance (ANOVA) was used to analyze the differences between the tested samples and untreated controls, the statistically significant difference was indicated at *P* value ≤ 0.05 .

Results and discussion

Antimicrobial resistance by various microbial species associated with the development of serious diseases. So, proper observation and identification measures should be conducted for controlling the current unacceptable antimicrobial resistance scenario. The fast and effective *S. aureus* identification is essential for routine microbiology laboratories testing. In our study, 42 *S. aureus* isolates were phenotypically identified based on their typical bacteriological features. These isolates were able to grow and ferment the mannitol sugar in MSA,

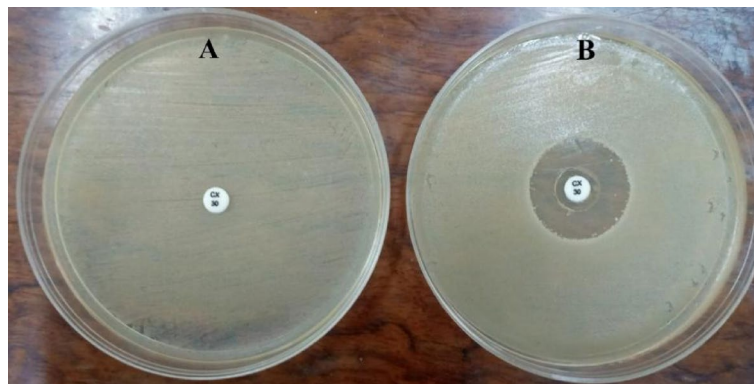


Fig. 1. Disc diffusion assays showing cefoxitin disc (30 µg) effect on representative MRSA (A) and MSSA (B) clinical isolates.

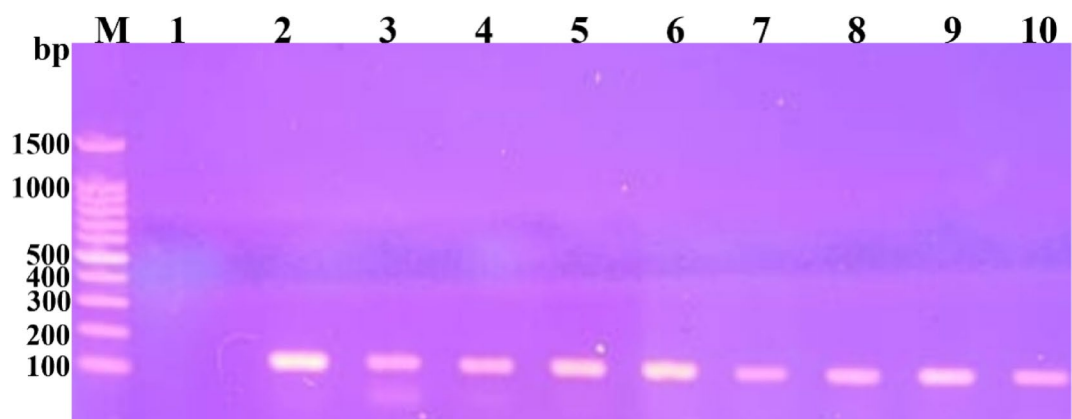


Fig. 2. Representative gel electrophoresis of the PCR-based *mecA* gene magnification products. Lanes, M; 100 bp DNA ladder, 1; negative control, 2–10; pointed to positive *mecA* gene results with specific bands, at about 147 bp, in phenotypically identified MRSA isolates 1–9, respectively.

produce distinctive golden yellow colonies when cultured on nutrient agar, and cause β -hemolysis on blood agar. Microscopically, all isolates were Gram-positive cocci with predictable grape-like arrangement. Biochemically, these isolates were able to produce oxidase, catalase, DNase, and coagulase enzymes. In a related research conducted by Shahzad et al.⁷⁴, *S. aureus* isolates growing on MSA were preliminary identified based on the catalase and coagulase tests and hemolysin production. Further confirmation was based on their morphological characteristics observed on various culture media and biochemical properties. Also, Minhas et al.⁷⁵ identify *S. aureus* clinical isolates because of their cultural, microscopic, and biochemical characteristics.

According to the oxacillin resistant screening agar test results, it was noticeable that 27 *S. aureus* isolates were grown on MSA/oxacillin discriminating media and consequently classified as oxacillin resistant. Conversely, the other 15 *S. aureus* isolates were identified as oxacillin sensitive since they failed to grow on the selective media. Interestingly, the Clinical Laboratory Standard Institute guidelines (CLSI, 2023) interpretation of cefoxitin disc diffusion test results clarified that only 26/27 the obtained oxacillin resistant *S. aureus* isolates showed $\text{IZD} \leq 21$ mm and confirmed as belonged to MRSA phenotype while the remaining oxacillin resistant *S. aureus* isolate (1/27) showed $\text{IZD} \geq 22$ mm and recorded as MSSA. On the other hand, the 15 oxacillin sensitive isolates exhibited $\text{IZD} \geq 22$ mm and subsequently definitely recorded as MSSA (Fig. 1). In similar studies, $\text{IZD} \leq 21$ mm around cefoxitin disc was reasoned for phenotypic MRSA detection⁷⁶.

At the molecular side, PCR recognition of the expected band for *mecA* gene at approximately 147 bp (Fig. 2), in only phenotypically categorized MRSA isolates, indicates their confirmed genotypic identification. In similar study conducted in Egypt, *mecA* gene was harbored in all phenotypically identified MRSA and not detected in their tested MSSA⁷⁷. Also, the *mecA* gene detection was the basis for genotypic differentiation between MRSA and MSSA clinical isolates⁷⁸. The positive correlation between the cefoxitin disc test findings and presence of *mecA* gene illustrated the usefulness of diffusion test as a quick and cost-effective screening method for MRSA identification and the importance of molecular technique for MRSA confirmation.

Biogenic synthesis and characterization of ZnO NPs

Biologically derived ZnO NPs offer significant advantages over traditional synthesis methods, including reduced production costs, enhanced biocompatibility, and lower toxicity⁷⁹. Recently, biogenic ZnO NPs have shown hopeful applications in antibacterial and biomedical fields^{27,80}. Our study demonstrates that the cell-free filtrate of *Mucor racemosus* can efficiently produce ZnO NPs, achieving higher yields, minimized aggregation, and the generation of smaller NPs⁸¹. Observing a color change in the biomass filtrate, likely due to metal precursor interactions, was an early indicator of ZnO NP formation. Similar approaches have been adopted by Kalpana et al.⁸², who used *Aspergillus niger* culture filtrates, while Abdelhakim et al.⁸³ utilized *Alternaria tenuissima* supernatants for ZnO NP biosynthesis. Additionally, *Phanerochaete chrysosporium* has been applied by Sharma et al.⁸⁴, and Abdelkader et al.⁸⁵ used *Aspergillus niger* for ZnO NP biofabrication. Numerous studies also highlight using various biological sources, including plant extracts and microbial media, to biosynthesize ZnO NPs^{86–88}.

The biosynthesized ZnO NPs were characterized using physicochemical analyses as well as the topographic assessments. The obtained UV–vis spectrum of biogenic ZnO NPs presented in Fig. 3. An initial visual sign of ZnO NP formation was a color change, resulting in a white precipitate. This observation was further supported by UV–vis spectrophotometry, which offered preliminary confirmation of ZnO NP synthesis, with distinctive peak at 320 nm in the spectra. Similarly, Kalpana et al.⁸² detected comparable ZnO NPs peak at 320 nm. Additionally, Mohd Yusof et al.⁸⁶ recorded surface plasmon resonance (SPR) values of 349 nm and 351 nm for ZnO NPs synthesized from *Lactobacillus plantarum* TA4 using cell biomass and supernatant, respectively. Umar et al.⁸⁸ reported that ZnO NPs typically exhibit a UV–vis absorption peak around 370 nm, while Al-Askar et al.⁸⁹ recorded an ecologically synthesized ZnO NPs with highest SPR peak at 360 nm using *Pluchea indica* plant. The use of *Mucor racemosus* for large-scale nanoparticle production is a sustainable alternative to traditional methods, offering environmental benefits such as reduced hazardous waste, lower energy consumption, and minimal greenhouse gas emissions. By utilizing natural biomolecules and renewable substrates like agricultural waste, this approach promotes a circular economy and resource efficiency. The resulting nanoparticles are biocompatible and biodegradable, reducing environmental persistence and contamination risks. Aligning with green chemistry principles, this method highlights the potential for a more sustainable and eco-friendly nanotechnology industry.

The particle size and morphology of biosynthesized ZnO NPs using *Mucor racemosus* were examined utilizing TEM examination. The TEM image (Fig. 4A) showed predominantly spherical ZnO NPs with distribution of particle size in the range of 15–55 nm, and a mean size of approximately 40 nm. The NPs were uniformly dispersed (Fig. 4A) with no evidence of aggregation or clumping. In comparison, *Aspergillus sojae*-derived ZnO NPs, synthesized using mycelial-cell free filtrate, formed nanoclusters with multiple shape, such as oval

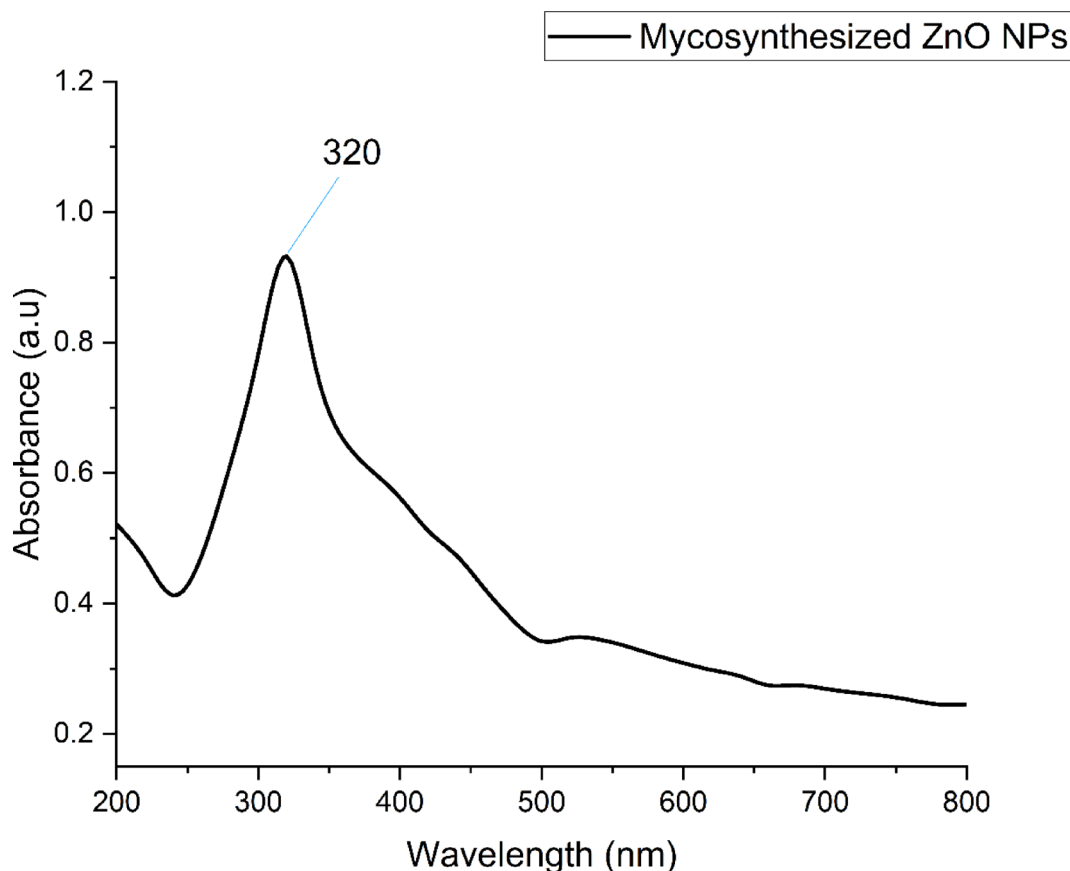


Fig. 3. The UV–vis spectrophotometer of biosynthesized ZnO NPs.

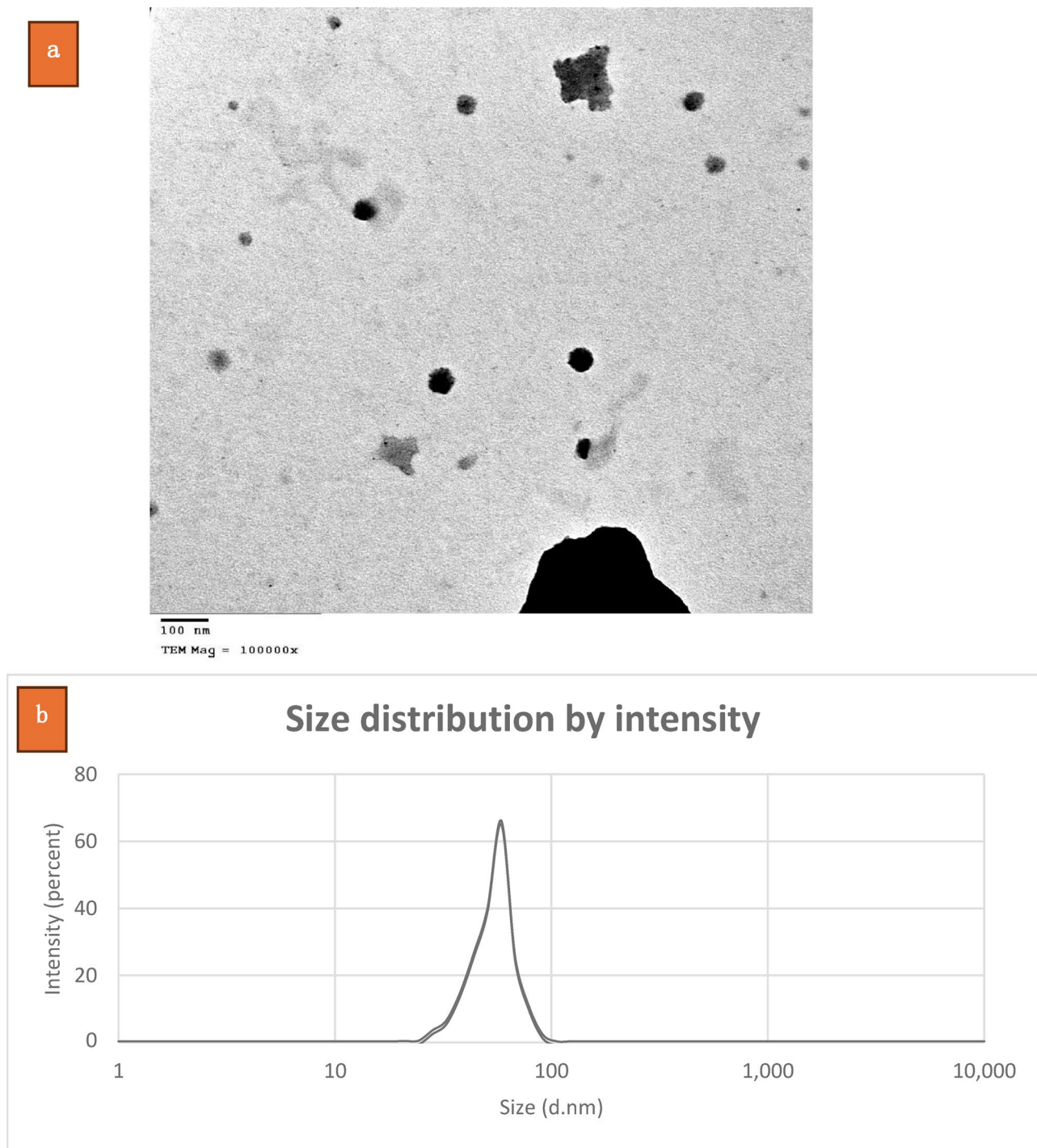


Fig. 4. Myco-synthesized ZnO NPs TEM image (A) and DLS (B).

and quasi-spherical⁶⁵. Mohd Yusof et al.⁸⁶ reported that high-resolution TEM (HR-TEM) images of ZnO NPs synthesized from *Lactobacillus plantarum* supernatants with flower-like shape in case of NPs-CFS while the NPs-CB revealed irregular morphology, and the NPs size was 291.1 nm and 191.8 nm, respectively. Also, another study carried out by Salih et al.⁹⁰ observed spherical ZnO NPs in the range of 16–35 nm. Abdelhakim et al.⁸³ study similarly demonstrated biosynthesized spherical shaped ZnO NPs by *Alternaria tenuissima* with mean size of 15.45 nm. Moreover, Fouda et al.⁹¹ reported minor aggregation amongst biosynthesized ZnO NPs that were spherical in shape with size range of 10–45 nm and average NPs size of about 25 nm.

A comparative analysis of biosynthesized nanoparticles reveals significant variations in size and morphology depending on the biological source used. ZnO nanoparticles synthesized using *Aspergillus niger* exhibited a compact rod-like and clustered structure, with a size range of 80–130 nm⁹². In contrast, ZnO nanoparticles derived from *Moringa oleifera* leaf extract were significantly smaller, with an average diameter of 25–30 nm,

and displayed a spherical morphology without aggregation⁹³. Silver nanoparticles (AgNPs) synthesized using *Azadirachta indica* showed a spherical shape with a particle size of approximately 33 nm⁹⁴. Similarly, gold nanoparticles (AuNPs) synthesized using *Bacillus subtilis* ANR 88 exhibited a predominantly spherical morphology, with a much smaller size range of 4–18 nm⁹⁵. Furthermore, nickel oxide nanoparticles (NiO NPs) produced from *Sargassum wightii* displayed cubic and hexagonal structures with an average crystallite size of 15–20 nm⁹⁶.

These findings highlight that the size and morphology of biosynthesized nanoparticles are strongly influenced by the biological system used for synthesis. ZnO NPs obtained from *Moringa oleifera* exhibit a smaller, well-dispersed spherical shape, which may enhance their bioavailability and surface reactivity, making them suitable for biomedical applications. In contrast, *Aspergillus niger*-derived ZnO NPs, with their larger and more compact rod-like structure, may offer advantages in photocatalytic and environmental applications. Silver and gold nanoparticles, being smaller in size and highly uniform in morphology, are widely recognized for their antimicrobial and biomedical potential. Meanwhile, the cubic and hexagonal nature of NiO NPs suggests distinct physicochemical properties that could be beneficial in catalytic and electronic applications. This comparative evaluation provides valuable insights into how the choice of biological synthesis method can tailor the structural characteristics of nanoparticles for specific applications.

Additionally, TEM analysis of ZnO NPs produced by *Phanerochaete chrysosporium* revealed NPs size in the range of 5–200 nm, as reported by Sharma et al.⁸⁴. Examination of colloidal solution based on DLS was utilized for determination of ZnO NPs size and distribution. Insights into the influence of stabilization, the surrounding environment, as well as the capping agents are crucial factors that control the NPs hydrodynamic diameter⁹⁷. The sensitivity of DLS to the aggregate's existence make this technique particularly effective in monitoring early-stage aggregation. Our DLS results revealed biosynthesized ZnO NPs average size about 59 nm (66% volume) (Fig. 4B). In a similar study, Omran and Kwang-Hyun⁶⁵, reported biogenic ZnO NPs with average size of 276.7 nm and polydispersity index (PDI) value equal 0.101. Additionally, Abdelkader et al.⁸⁵ reported an average hydrodynamic diameter of 225.46 ± 3.27 nm for the ZnO NPs, with a PDI value about 0.186 ± 0.05 . The PDI value provides insight into the uniformity of the colloidal NPs, with a lower PDI indicating a more homogeneous distribution⁹⁸. In our study, the recorded PDI value of 0.186 signifies a high degree of homogeneity in the NPs population.

The stability of ZnO NPs under physiological conditions is a crucial factor determining their biomedical applicability, particularly in drug delivery, antimicrobial therapies, and tissue engineering⁹⁹. Stability in biological fluids such as blood, plasma, and intracellular environments ensures prolonged circulation time, bioavailability, and controlled interactions with target cells¹⁰⁰. Although direct stability assessments were not conducted in this study, insights from previous literature suggest that biosynthesized ZnO NPs often exhibit enhanced stability due to the presence of capping agents derived from biological extracts. These natural stabilizers prevent aggregation, improve dispersion, and modulate surface charge, which collectively influence their interactions in biological environments¹⁰¹. One key factor influencing nanoparticle stability is the zeta potential, which determines electrostatic repulsion between particles. Studies have indicated that biosynthesized ZnO NPs with a sufficiently high zeta potential ($> \pm 30$ mV) maintain better colloidal stability in physiological conditions, reducing the likelihood of aggregation^{102,103}. Additionally, ZnO NPs synthesized via green methods often feature biomolecule coatings that enhance stability by preventing aggregation and reducing protein corona formation, which can affect cellular interactions and toxicity¹⁰⁴. Their solubility is pH-dependent, with slight dissolution in acidic conditions leading to controlled Zn^{2+} ion release, beneficial for antimicrobial and therapeutic applications. However, excessive dissolution may affect long-term stability, requiring further optimization¹⁰⁵. Based on these factors, the biosynthesized ZnO NPs in this study are expected to exhibit reasonable stability under physiological conditions due to biomolecular capping.

To investigate the interactions between the active metabolites of *Mucor racemosus* and the created ZnO NPs, the FTIR spectrum was analyzed. The fungal filtrate, containing proteins and enzymes, have fundamental function during NPs synthesis and stabilization¹⁰⁶. The spectra of FTIR for biosynthesized ZnO NPs (Fig. 5A) were recorded across the 400–4000 cm^{-1} wavenumber range. Notable absorption peaks were detected which include 3209, 2892, 1783, 1621, 1421, 1306, 1155, 1104, 1025, 892, 703, 597, and 505 cm^{-1} . These peaks represent specific functional groups including C–H stretching from CH_2 , C=O and C–O vibrations from COO^- groups, and O–H stretching associated with H_2O molecules⁹⁰. Additional bands indicative for primary amines and phenolic compounds were also identified. In ZnO NPs spectrum, a distinctive 703 cm^{-1} absorption peak was observed, potentially linked to NPs interaction and conjugation. Further analysis in Fig. 5A revealed the COO^- and O–H groups occurrence. Also, protein stretch was detected at 505 cm^{-1} , aligning with previous findings¹⁰⁷. In agreement with Omran and Kwang-Hyun⁶⁵, the peaks detected in the range of 400–1000 cm^{-1} were attributed to Zn–O bond vibrations in ZnO NPs. These observations are consistent with reports from other studies on ZnO NP biosynthesis^{82–84}.

The obtained XRD pattern of ZnO NPs, biosynthesized utilizing *Mucor racemosus*, displayed in Fig. (5B). Our results revealed crystalline structure of the biosynthesized hexagonal ZnO NPs. The XRD pattern showed characteristic peaks of diffraction related to 100, 002, 101, 102, 110, 103, 220, 112, and 201 planes, confirming ZnO NPs hexagonal phase. Specifically, nine distinct peaks of diffraction at 2θ angle of 31.8°, 34.5°, 36.4°, 47.6°, 56.5°, 63.0°, and 67.5° were detected. No peaks from impurities were detected, indicating that the ZnO NPs are of high purity (Fig. 5B). The most prominent peak at $2\theta = 36.4^\circ$ (101) corresponds to the primary facet, suggesting a well-ordered structure with minimal impurity content. The size of crystallite was estimated based on Scherrer equation, that depend on the full width at half maximum (FWHM) of the most intense peak at the plane 101. The biosynthesized ZnO NPs average crystallite size was found to be 45 nm. This observation agrees with previous studies, such as those by Omran and Kwang-Hyun⁶⁵, who identified Bragg reflections at 2θ values of 31°, 34°, 36°, 47°, 56°, 62°, 67°, 69°, and 77°, corresponding to specific ZnO lattice planes. Similarly, Venu

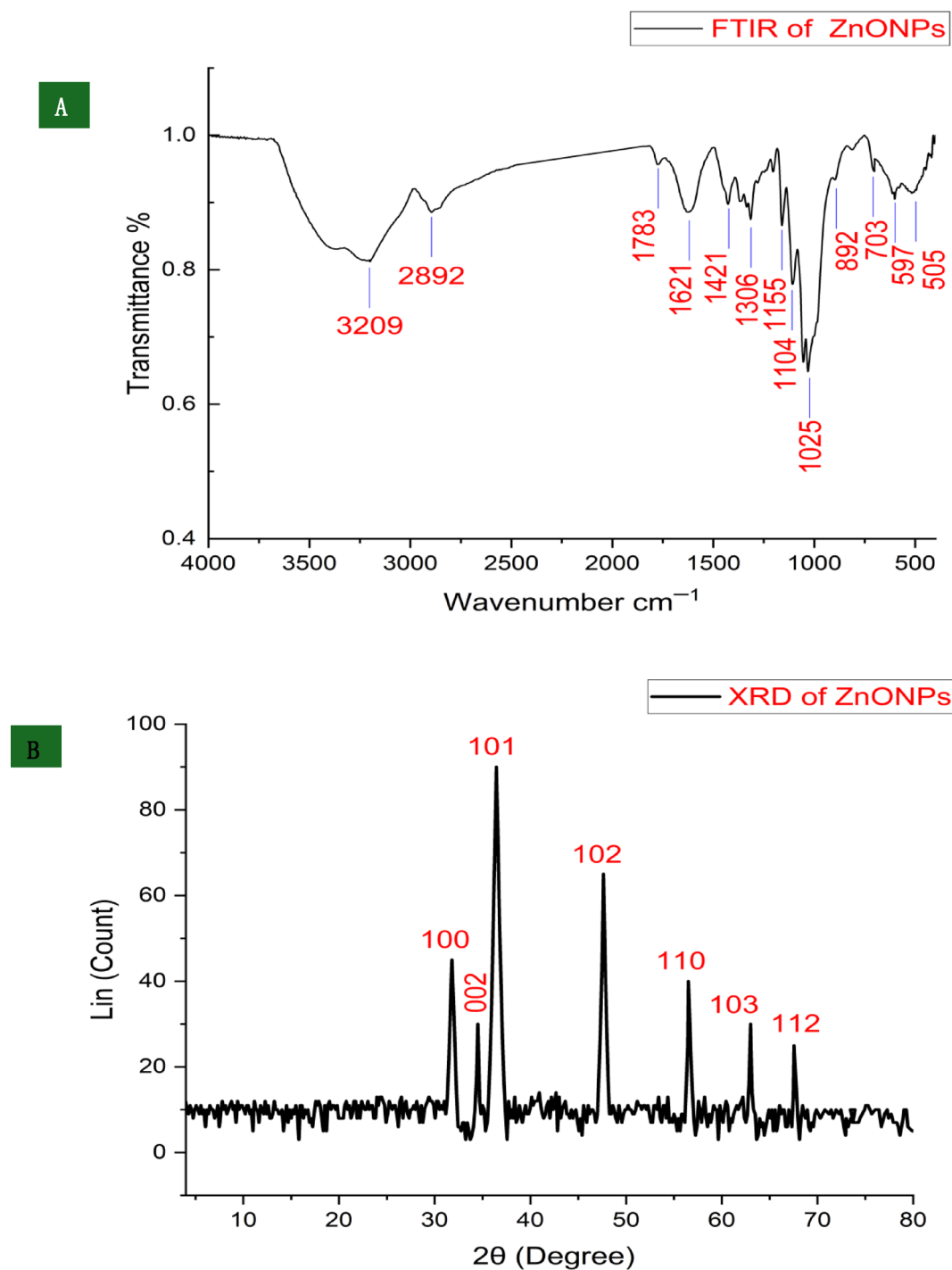


Fig. 5. Myco-synthesized ZnO NPs FTIR (A) and XRD (B) spectra.

Gopal and Kamila⁶⁶ calculated an average crystallite sizes of 23, 19, and 37 nm for ZnO synthesized from various salts of zinc including acetate, nitrate, and sulfate salt, respectively). Additionally, Batoo et al.¹⁰⁸ study reported crystallite size with a mean of about 39 nm for biogenic ZnO NPs synthesized using *Ganoderma multipileum*.

Anticancer activity

The biosynthesized ZnO NPs from fungi have shown promising anticancer effect based on their unique properties, including high surface area with enhanced activity. Fungal biosynthesis of ZnO NPs offers an ecofriendly method, leveraging the natural ability of certain fungi to reduce zinc ions into NPs¹⁰⁹. In the current study, the biosafety of myco-synthesized ZnO NPs was shown through evaluation of its cytotoxicity against Wi-38 normal cell line (Fig. 6A). The results revealed cell viability of 99.23, 98.8, 94.23, 81.86 and 66.76% based on

the exposed ZnO NPs concentrations including 7.81, 15.62, 31.25, 62.5 and 125 $\mu\text{g/mL}$, respectively. Moreover, IC_{50} of myco-synthesized ZnO NPs against Wi-38 cell line was 197.2 $\mu\text{g/mL}$.

According to these ZnO NPs biosafety findings, its anticancer effect was carried out at different concentrations in the range of 7.81–250 $\mu\text{g/mL}$ (Fig. 6B). Results showed promising anticancer effect of myco-synthesized ZnO NPs of 94.13, 81.63, 59.53, 32.16% upon exposure to concentration ranged from 31.25 to 250 $\mu\text{g/mL}$, respectively. Furthermore, the IC_{50} of about 51.4 $\mu\text{g/mL}$ for the myco-synthesized ZnO NPs was observed.

Previous studies reported that, ZnO NPs which synthesized by fungi have promising anticancer activity. Hammad et al.¹¹⁰ used *Fusarium chlamydosporum* for biosynthesis of ZnO NPs with anticancer potential toward CACO2 and HCT-116. Also, myco-synthesized ZnO NPs from *Aspergillus niger* showed promising anticancer activity against¹¹¹. Moreover, Gao et al.⁹² employed *A. niger* for biosynthesis of ZnO NPs that displayed anticancer activity against Hep-G2 cancerous cell line with IC_{50} 26.75 \pm 1.04 $\mu\text{g/mL}$.

Several mechanisms are involved in ZnO NPs anticancer properties. These NPs could induce cancer cells apoptosis in via disrupting mitochondrial function with caspases activation, leading to programmed cell death. Additionally, ZnO NPs produce reactive oxygen species (ROS), that cause oxidative stress associated with destruction of critical cellular components, ultimately promoting cell death¹¹². They also interfere with cell cycle progression, particularly causing arrest at the G1/S or G2/M phases, which hinders cancer cell proliferation. Furthermore, ZnO NPs can disrupt angiogenesis with consequent hindering of blood supply to the tumor cells through delaying of new blood vessels formation¹¹³. Collectively, these mechanisms highlight ZnO NPs' capacity as an effective tumor controlling agent for cancer treatments which offer a promising alternative for conventional therapeutic agents.

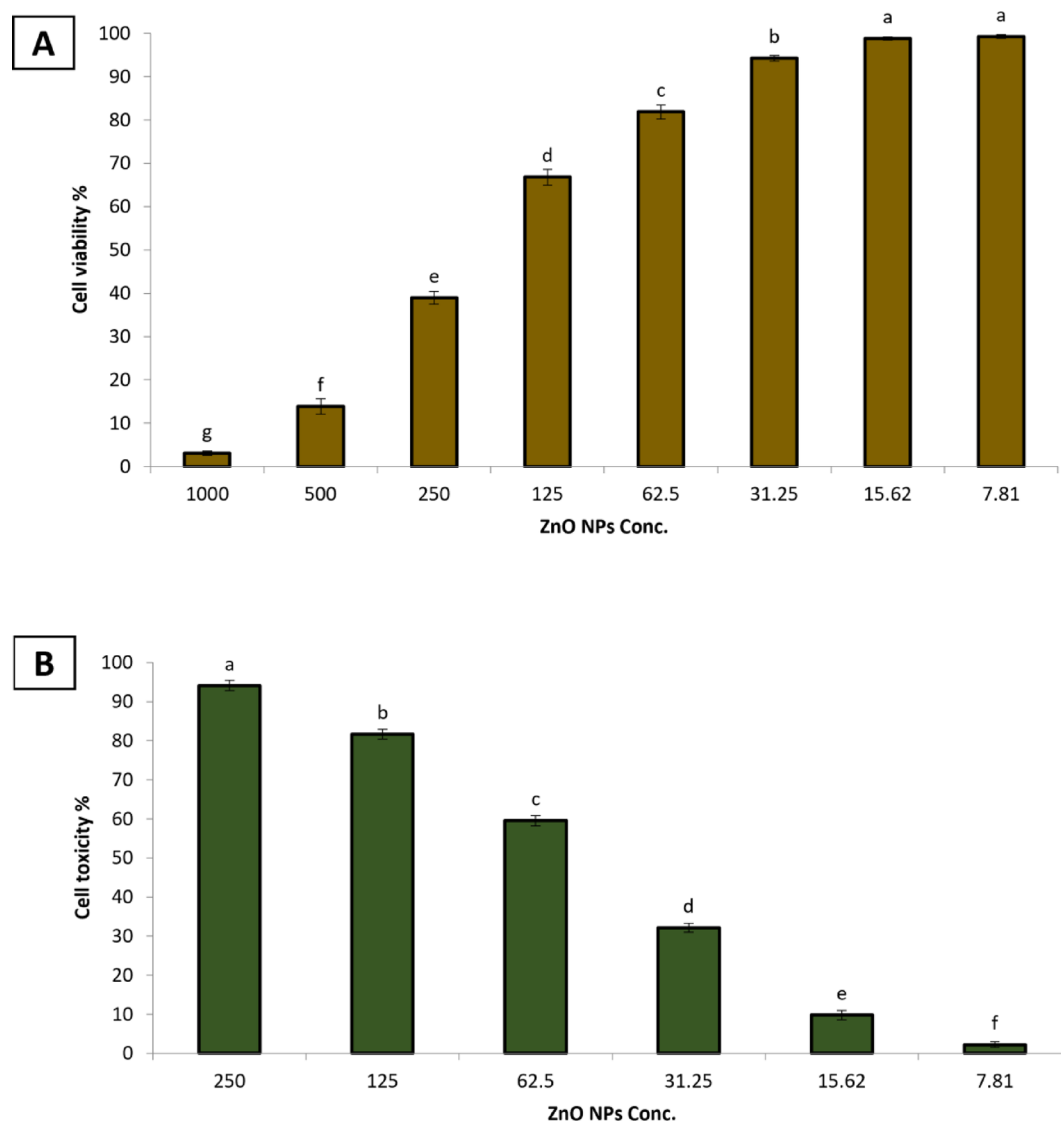


Fig. 6. Cytotoxicity of myco-synthesized ZnO NPs against Wi-38 normal (A) and Hep-G2 cancerous (B) cell lines.

Antioxidant activity

Nanoparticles have gained significant attention for their potential antioxidant activity, which is crucial in mitigating oxidative stress and related diseases. These nanoscale materials, including metal oxides, carbon-based NPs, and polymeric NPs, can scavenge free radicals, enhancing cellular defense mechanisms^{114,115}. In this study, the antioxidant activity of myco-synthesized ZnO NPs was noticeable (Fig. 7). Results revealed significant antioxidant activity of myco-synthesized ZnO NPs at 50, 100, and 200 µg/mL at a percentage of 41, 58.63, and 68.36%, respectively. Furthermore, IC_{50} of myco-synthesized ZnO NPs was 69.2 µg/mL.

These ZnO NPs antioxidant potential may be correlated to the scavenging of ROS, such as OH and H_2O_2 radicals, with consequent prevention of cellular destruction. Additionally, the ZnO NPs tiny size with high surface area enhance its contact with free radicals, effectively neutralizing them¹¹⁶. Also, these NPs could improve the endogenous antioxidant activity mediated by catalase and superoxide dismutase enzymes, which further bolsters the cell's defense against oxidative damage¹¹⁷. Moreover, ZnO NPs could lower the oxidative stress associated signaling pathways, promoting cellular survival and reducing inflammation¹¹⁸. This dual action of direct scavenging and enzymatic enhancement emphasizes the ZnO NPs potential in remedial applications targeted the prevention of disorders associated with oxidative stress. The antioxidant activity of ZnO NPs is primarily attributed to their ability to scavenge ROS and regulate oxidative stress pathways. ZnO NPs can interact with free radicals, reducing oxidative damage through electron transfer and radical neutralization mechanisms¹¹⁶. Additionally, they may enhance the activity of antioxidant enzymes such as superoxide dismutase (SOD) and catalase, which play a crucial role in mitigating cellular oxidative stress. The gradual release of Zn^{2+} ions also contribute to their protective effects by influencing cellular redox balance and promoting the expression of antioxidant defence mechanisms. These properties suggest that ZnO NPs have potential therapeutic applications in oxidative stress-related diseases, including neurodegenerative disorders, cardiovascular conditions, and inflammatory diseases. However, further studies are needed to optimize their stability, bioavailability, and safe dosage for biomedical applications¹¹⁹.

Antimicrobial activity

A remarkable interest have directed towards ZnO NPs due to their biomedical applications and antibacterial and antifungal activities¹²⁰. In the current study, microbiological assay based on agar diffusion (Fig. 8) illustrated the variable initial qualitative antibacterial efficacy of ZnO NPs (1000 µg/mL) against both MRSA and MSSA clinical isolates (Table 1). A noticeable wide range of IZD, 9 ± 0 to 34.7 ± 0.6 mm and 6 ± 0 to 33 ± 0 mm, was recorded against the tested MRSA and MSSA isolates, respectively. Fortunately, the obtained IZD were nearly comparable with vancomycin standard antibacterial agent that showed IZD range of 11 ± 0 to 33 ± 1.73 and 0 ± 0 to 31 ± 0 mm against the tested MRSA and MSSA isolates, respectively. Also, the calculated PI of ZnO NPs was 34.9–188.2% for MRSA and 53.3–166.4% for MSSA clinical isolates. Statistically, the findings showed the significant/insignificant difference of biogenic ZnO NPs activity against the tested MRSA and MSSA isolates. Statistically, the well diffusion assay findings showed inverse relationship of correlation coefficient (r) between the IZD caused by biogenic ZnO NPs activity and presence of *mecA* gene and the subsequent methicillin resistance which means a decrease in IZD with presence of *mecA* gene. As the calculated P value was 0.00071, this correlation was statistically significant. Furthermore, a negative correlation ($r = -0.0508$) was observed amongst vancomycin

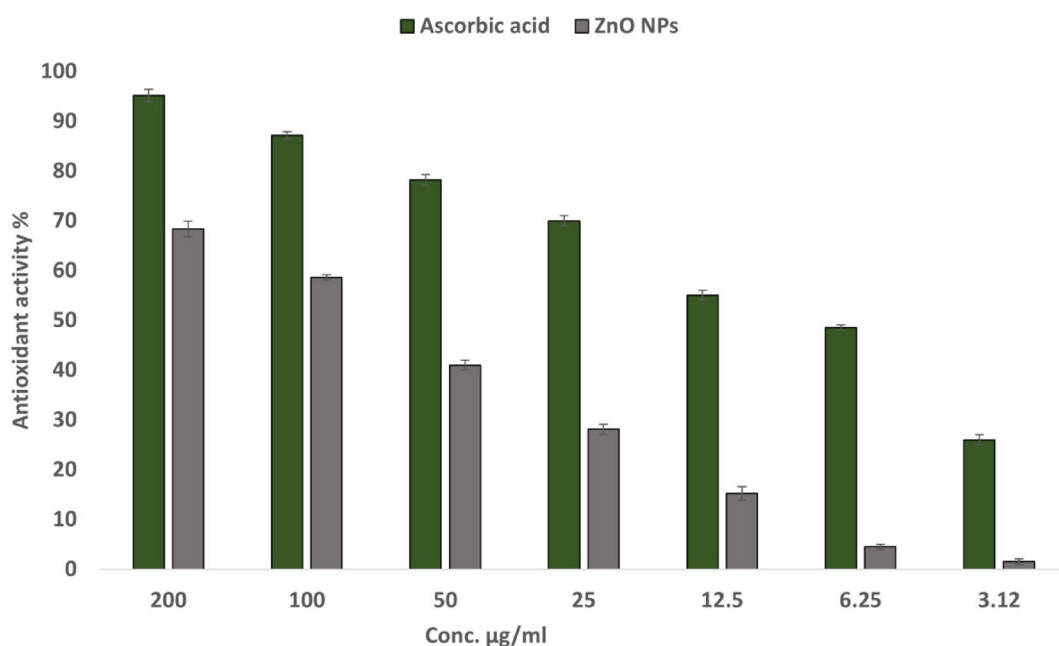


Fig. 7. Myco-synthesized ZnO NPs antioxidant potential as determined by DPPH method using concentrations ranged from 3.12 to 200 µg/mL.

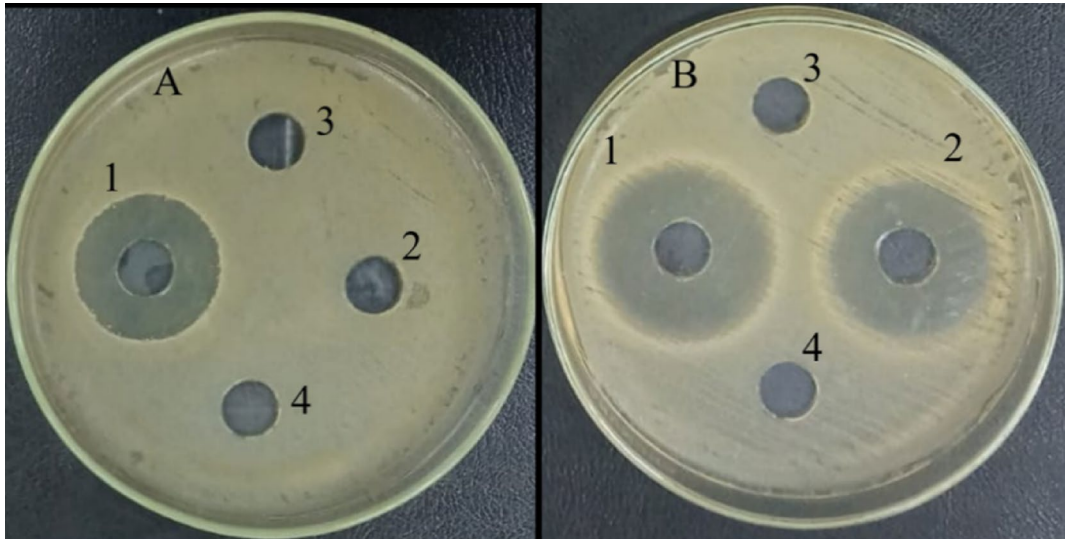


Fig. 8. Representative agar well diffusion assay showed variable MRSA (A) and MSSA (B) clinical isolates growth inhibitory effect by ZnO NPs 1000 µg/mL (well 1), vancomycin 50 µg/mL as a positive control (well 2), zinc acetate 1000 µg/mL (well 3), and DMSO 8% as a negative control (well 5).

Isolates ^a	Character			Isolates	Character		
	Agar well diffusion assay				Agar well diffusion assay		
	ZnO NPs	C	PI (%)		ZnO NPs	C	PI (%)
	IZD (mm)				IZD (mm)		
RS ₁	16.7 ± 0.6	18 ± 0	92.8	RS ₂₂	20.7 ± 0.6	11 ± 0	188.2
RS ₂	22.7 ± 0.6	20.67 ± 0.58	109.8	RS ₂₃	15.7 ± 0.6	15.33 ± 1.15	102.4
RS ₃	12 ± 1	21 ± 0	57.1	RS ₂₄	9 ± 0	12.33 ± 1.15	73
RS ₄	20.3 ± 0.6	24 ± 0	84.6	RS ₂₅	30.7 ± 1.2	27.67 ± 0.58	110.9
RS ₅	27.7 ± 0.6	32.67 ± 0.58	84.9	RS ₂₆	34.7 ± 0.6	33 ± 1.73	105.1
RS ₆	18.3 ± 0.6	15.33 ± 0.58	119.4	SS ₁	32.3 ± 1.2	31 ± 0	104.2
RS ₇	22.3 ± 0.6	20 ± 0	111.5	SS ₂	28 ± 0	28.67 ± 0.58	97.3
RS ₈	25.3 ± 0.6	21.67 ± 0.58	116.7	SS ₃	30 ± 1	28 ± 0	107.1
RS ₉	25.7 ± 0.6	22 ± 0	116.8	SS ₄	22.7 ± 0.6	27.33 ± 0.58	83.1
RS ₁₀	17 ± 0	23.67 ± 0.58	71.8	SS ₅	7.7 ± 0.6	10 ± 0	77
RS ₁₁	18.7 ± 0.6	19.33 ± 0.58	96.7	SS ₆	12 ± 0	21.67 ± 0.58	55.4
RS ₁₂	11.3 ± 0.6	32.33 ± 0.58	34.9	SS ₇	27 ± 0	25.67 ± 0.58	105.2
RS ₁₃	26.3 ± 1.2	18.67 ± 0.58	140.9	SS ₈	33 ± 0	25 ± 0	132
RS ₁₄	15.7 ± 0.6	20.67 ± 0.58	75.9	SS ₉	23.3 ± 0.6	14 ± 0	166.4
RS ₁₅	25.7 ± 0.6	15.33 ± 0.58	167.6	SS ₁₀	8 ± 0	15 ± 0	53.3
RS ₁₆	14.3 ± 0.6	15.67 ± 0.58	91.2	SS ₁₁	18.3 ± 0.6	19.33 ± 0.58	94.7
RS ₁₇	23.3 ± 1.2	20.67 ± 0.58	112.7	SS ₁₂	20.3 ± 1.2	8 ± 0	128.7
RS ₁₈	27.7 ± 0.6	20 ± 0	138.5	SS ₁₃	31.3 ± 0.6	27.67 ± 0.58	113.1
RS ₁₉	19.7 ± 0.6	19.67 ± 0.58	100	SS ₁₄	6 ± 0	11 ± 0	54.5
RS ₂₀	24.3 ± 0.6	29.33 ± 0.58	82.8	SS ₁₅	8 ± 0	12.33 ± 0.58	64.9
RS ₂₁	16.7 ± 0.6	20 ± 1	92.59	SS ₁₆	27.7 ± 0.6	30.33 ± 0.58	91.3

Table 1. ZnO NPs activity against MRSA and MSSA isolates from well diffusion assay. ^a RS₁-RS₂₆: MRSA clinical isolates (1–26), SS₁-SS₁₆: MSSA clinical isolates (1–16) ZnO NPs: zinc oxide nanoparticles, C: vancomycin, IZD; inhibition zone diameter, and PI; percent inhibition.

susceptibility (measured as an IZD) and methicillin resistance in *S. aureus*. However, this correlation was not statistically significant ($P=0.2159$).

In Abo-Shama et al.¹²¹ study, different ZnO NPs concentrations exhibited promising initial activity against *S. aureus* where the largest IZD (26.0 ± 0.57 mm) was caused by 170 µg/mL ZnO NPs. Also, the agar diffusion technique for screening of ZnO NPs antibacterial activity revealed a dose dependent antibacterial effect with

maximum cytotoxicity, $IZD = 19.0 \pm 0.7$ mm and 18.25 ± 0.5 mm, against MSSA and MRSA, respectively at ZnO NPs concentration of $2000 \mu\text{g/mL}$ ¹²². Similarly, the obtained IZD of ZnO NPs against the tested MRSA and MSSA isolates were in the range of 14 to 24 mm¹²³. Parallel findings of antimicrobial susceptibility of ZnO NPs ($5 \mu\text{g/mL}$), determined by disc diffusion assay, was illustrated the ZnO NPs inhibitory effect on the growth of Gram-positive bacteria including MRSA strains with IZD of 11–14 mm¹²⁴. These findings illustrate the initial antibacterial activity against the tested MRSA and MSSA strains. Statistical analysis of the treatment outcomes for MRSA isolates using ZnO NPs versus the control (vancomycin) revealed no significant differences, with a *P* value of 0.8643. Similarly, the treatment of MSSA isolates showed no statistically significant differences, yielding a *P* value of 0.9842.

Quantitative antimicrobial activity

Zinc oxide NPs are one of the considerably used nanomaterials for healthcare applications due to their biodegradability and tunable chemical and physical properties¹⁰⁴. Additionally, ZnO NPs represent promising material for biomedical research, especially antimicrobial potential¹²⁵. In our study, the quantitative broth microdilution assay (Fig. 9) clarified the potent capability of biogenic ZnO NPs for growth inhibitory effect on the tested MRSA and MSSA isolates (Table 2). The obtained MIC of biogenic ZnO NPs was ranged from 32 to $512 \mu\text{g/mL}$ against the tested MRSA and MSSA isolates. Also, the MBC of ZnO NPs towards MSSA strains were in lower range of 32– $1024 \mu\text{g/mL}$ than its MBC range, 128– $1024 \mu\text{g/mL}$, against the MSSA. Statistical analysis of the MIC values for MRSA and MSSA strains demonstrated no significant differences between the two groups,

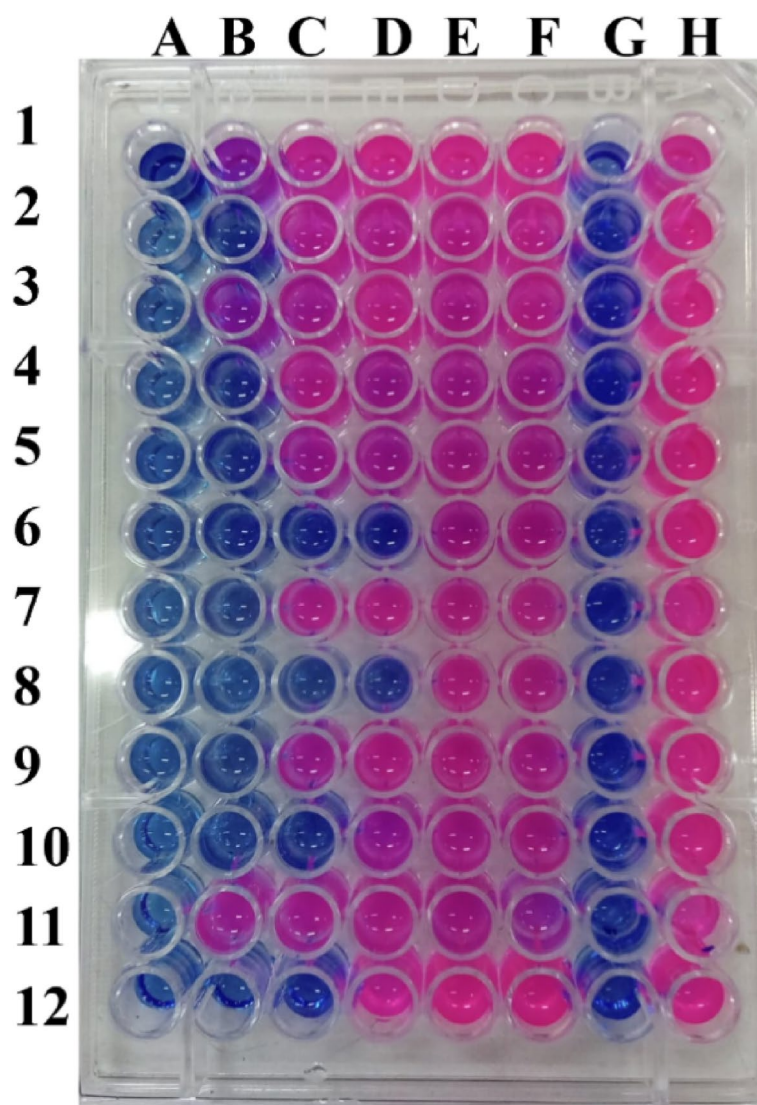


Fig. 9. Broth microdilution assays showing variable growth inhibiting effect of ZnO NPs. Rows 1 and 2 correspond to representative MRSA clinical isolates number 25 and 26, respectively while rows 3 and 12 correspond to representative MSSA clinical isolates number 1 and 10, respectively. Columns from A to F represent twofold ZnO NPs serial dilution ranged from 512 to $16 \mu\text{g/mL}$. The negative and positive control tests are represented by column G and H, respectively.

Isolates ^a	Character				Isolates	Character			
	ZnO NPs broth microdilution assay against MRSA					ZnO NPs broth microdilution assay against MSSA			
	MIC	MBC	MIC index	Antibiosis effect		MIC	MBC	MIC index	Antibiosis effect
µg/mL		µg/mL							
RS ₁	256	512	2	Bactericidal	RS ₂₂	128	256	2	Bactericidal
RS ₂	128	512	4	Bacteriostatic	RS ₂₃	128	512	4	Bacteriostatic
RS ₃	256	512	2	Bactericidal	RS ₂₄	512	512	1	Bactericidal
RS ₄	128	128	1		RS ₂₅	64	512	8	Bacteriostatic
RS ₅	32	32	1		RS ₂₆	64	256	4	
RS ₆	128	256	2		SS ₁	128	256	2	Bactericidal
RS ₇	128	256	2		SS ₂	32	128	4	Bacteriostatic
RS ₈	32	256	8		Bacteriostatic	SS ₃	128	256	2
RS ₉	32	128	4	SS ₄		64	128	2	
RS ₁₀	128	128	1	Bactericidal	SS ₅	256	1024	4	Bacteriostatic
RS ₁₁	128	512	4	Bacteriostatic	SS ₆	32	128	4	
RS ₁₂	512	1024	2	Bactericidal	SS ₇	128	256	2	Bactericidal
RS ₁₃	32	128	4	Bacteriostatic	SS ₈	32	128	4	Bacteriostatic
RS ₁₄	128	512	4		SS ₉	128	512	4	
RS ₁₅	64	512	8		SS ₁₀	64	128	2	Bactericidal
RS ₁₆	256	512	2	Bactericidal	SS ₁₁	256	512	2	
RS ₁₇	64	256	4	Bacteriostatic	SS ₁₂	512	1024	2	Bacteriostatic
RS ₁₈	64	128	2	Bactericidal	SS ₁₃	64	512	8	
RS ₁₉	128	256	2		SS ₁₄	512	1024	2	Bactericidal
RS ₂₀	64	128	2		SS ₁₅	512	512	1	
RS ₂₁	128	512	4	Bacteriostatic	SS ₁₆	128	512	4	Bacteriostatic

Table 2. ZnO NPs inhibitory concentrations against MRSA and MSSA clinical isolates. ^a RS₁-RS₁₂: MRSA clinical isolates (1–12), MIC; minimum inhibitory concentration, MBC; minimum bactericidal concentration, and T_{index}; therapeutic index.

with a *P* value of 0.359. This indicates that the observed variations in MIC values are likely attributable to random chance rather than a true difference in susceptibility between the MRSA and MSSA strains. Furthermore, variable biogenic ZnO NPs bacteriostatic or bactericidal antibiosis effect were expected from the recorded 1–8 tolerance level for each tested MRSA and MSSA isolate. Our observations revealed a positive correlation value ($r=0.1418$) with statistically insignificance between the bacteriostatic or bactericidal activity of ZnO NPs and methicillin resistance (*mecA* gene existence) with $P=0.4416$. These observations confirm the insignificant difference of biogenic ZnO NPs activity against the tested MRSA and MSSA isolates. Which means a more bacteriostatic activity was observed with methicillin resistance or occurrence of *mecA* gene.

In related research, high ZnO NPs bactericidal effect was noted against MRSA with an equal MIC and MBC. On the other hand, much higher activity was reported against their tested MSSA¹²⁶. Also, a similar study finding recorded ZnO NPs MIC of 1 and 2 mg/ml and MBC of 0.5 and 1.5 mg/ml for MRSA and MSSA, respectively¹²². Our results were also in accordance with Riahi et al.¹²⁷. research that described an equal ability of ZnO NPs for growth inhibition towards MRSA and MSSA. According to their calculated tolerance level, their ZnO NPs were classified as bactericidal agent against their tested MRSA and MSSA isolates. In another related study, Abdelraheem et al.¹²⁸ recorded MICs of ZnO NPs ranged from 128 to 2048 µg/mL amongst different antimicrobial resistant *S. aureus* isolates. Also, Khan et al.¹²⁹ reported ZnO NPs with MIC of 200 µg/mL towards MRSA strains of. As well, ZnO NPs with MIC and MBC of 31.25 µg/mL and 125 µg/mL, were recognized for *S. aureus* isolates, respectively¹³⁰. The different inhibitory concentrations of ZnO NPs, which indicate their variable activity against MRSA and MSSA, could be due to the preparation method and NPs size which affects their efficacy. However, the recorded low MIC, MBC, and tolerance level of ZnO NPs against MRSA and MSSA suggest their successful potential for treating infections associated with antimicrobial resistance bacterial phenotype. The correlated MIC, MBC, and tolerance level of ZnO NPs against MRSA and MSSA illustrate their overcoming of some resistant mechanisms in MRSA.

Biofilm destructive assay

Biofilms creation represent a crucial mechanism in numerous bacterial infections that basically responsible for more than 80% of bacterial associated humans’ disorders. *S. aureus* characterized by potent extracellular matrix or biofilm formation which contain proteins, nucleic acids, and carbohydrates that allow their survival and spreading. So, alternative techniques for controlling these humans’ bacterial diseases is a critical requirement. Recently, antibacterial effects based on metallic NPs, such as ZnO-NPs, emerged as an efficient approach for fighting bacterial biofilm drug resistance^{122,131}.

In our study, the CV staining assay illustrates the different ability of the tested MRSA and MSSA to biosynthesize variable biofilm degree (Fig. 10). Consequently, the tested MRSA isolates were classified into non (9/26; 34.6%), weak (6/26; 23.1%), moderate (5/26; 19.2%), and strong biofilm former (6/26; 23.1%). On the other hand, the tested MSSA isolates were classified into non (9/16; 56.25%), weak (4/16; 25%), moderate (1/16; 6.25%), and strong biofilm former (2/16; 12.5%). Statistically, analysis of findings CV assay discovered positive relationship ($r=0.26422$) between the capability for biofilm creation in *S. aureus* isolates and their methicillin resistance however this correlation was found to be statistically insignificant ($P=0.0945$).

Also, this assay demonstrated the biogenic ZnO NPs eradication potential on MRSA and MSSA biofilm. The MIC of the ZnO NPs reduced the exposed MRSA and MSSA preformed biofilm in a range of 23.24–73.96% and 6.63–74.1%, respectively (Fig. 11). Statistically, the negative correlation ($r=-0.1094$) between ZnO NPs biofilm eradication potential and methicillin resistance indicated an inverse relationship between biofilm clearance and presence of *mecA* gene or methicillin resistance. This correlation illustrated insignificance ($P=0.6106$). The results revealed high biogenic ZnO NPs activity against the preformed MSSA biofilm. Furthermore, a significant inverse correlation was observed between biofilm formation potential by *S. aureus* and biofilm clearance by biogenic ZnO NPs ($r=-0.1085$).

Our findings were in accordance with related research in which the biogenic ZnO NPs eradicate MRSA ATCC 33,591 biofilm in a concentration reliant way and maximum biofilm reduction ($75.79 \pm 0.785\%$) at $25 \mu\text{g/mL}$ ZnO NPs¹³². In other related antibiofilm studies, ZnO NPs revealed optimum inhibition in microbial biofilm formation. The MRSA cultured for 24 h in presence of ZnO NPs ranged from 0.25 to 2 mg/ml showed decreased biofilm formation in the range of 3–51%¹³². Also, the antibiofilm effect of ZnO-NPs ($54 \mu\text{g/mL}$) against MRSA ATCC 43,300 showed considerable biofilm reduction of $77.35 \pm 2.67\%$ ¹³³. Similarly, Lahiri et al.¹³⁴ work demonstrated an effective destruction of the major oral bacterial biofilms produced by *Alcaligenes faecalis* and *Porphyromonas gingivalis* after treatment with ecofriendly-synthesized ZnO NPs by $92.27 \pm 1.22\%$ and $95.27 \pm 1.28\%$, respectively. Also, zinc imidazole framework NPs (ZIF-8 NPs) revealed both MRSA biofilm formation suppression and biofilm eradication capabilities through reduction of various adhesion-related proteins expression¹³⁵. Inclusively, the findings illustrated the biogenic ZnO NPs effective inhibition or eradication ability and consequent elimination of bacterial biofilm. This ability for bacterial biofilm degradation could be due to debilitation of the extracellular polymeric structural components of the biofilm including proteins and carbohydrates that provides the biofilm with adequate strength. Additionally, this antibiofilm activity could be due to ROS production that considerably interfere with biofilm integrity via interrupting the bacterial exopolysaccharide biosynthesis.

Conclusions

This study successfully demonstrated ZnO NPs mycosynthesis using *Mucor racemosus*, highlighting an ecological and helpful method for NPs biosynthesis. Characterization techniques established their spherical shape and suitable diameter. These NPs exhibited significant anticancer activity against Hep-G2 cells and showed acceptable biosafety level towards Wi-38 normal cell line. Additionally, the antioxidant properties of the eco-

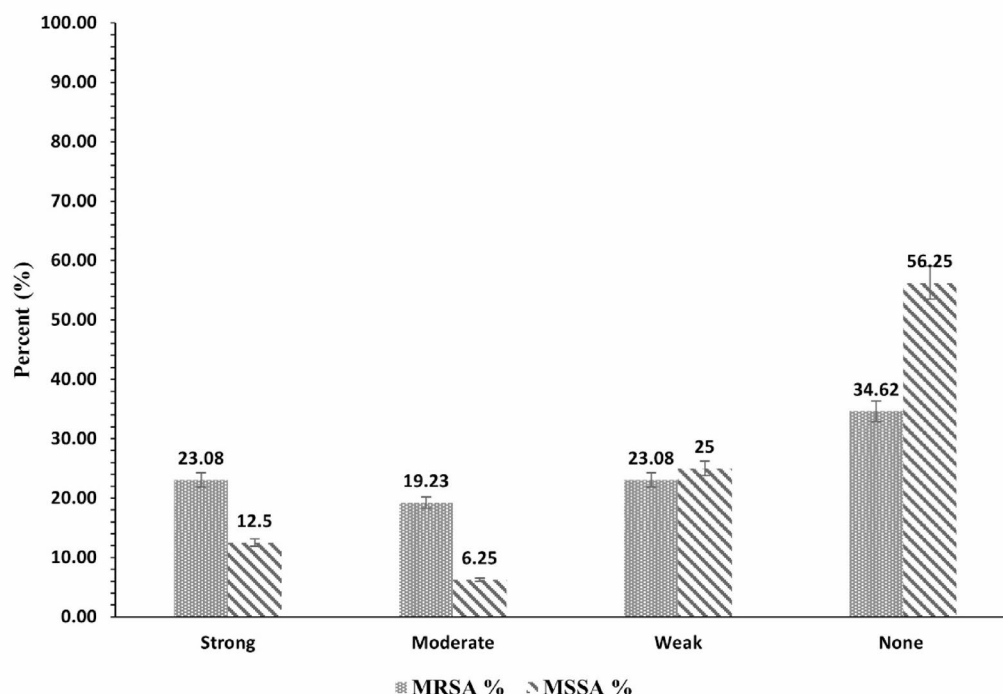


Fig. 10. Different biofilm categories represented MRSA and MSSA clinical isolates.

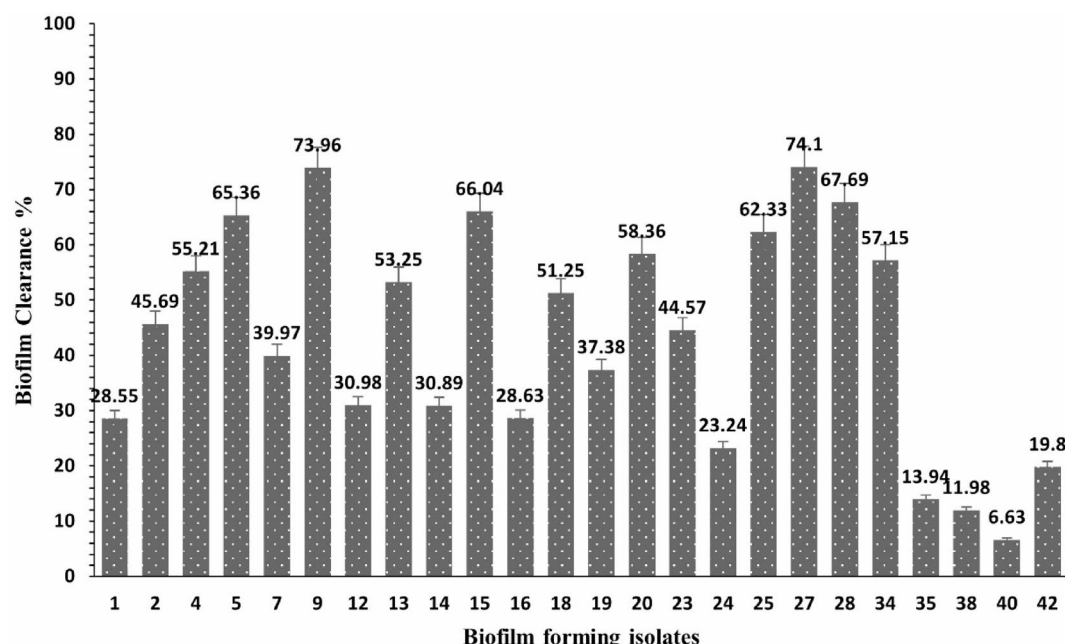


Fig. 11. Biofilm clearance rates by MIC ZnO NPs against biofilm forming MRSA (1–25) and MSSA (27–42) isolates.

friendly ZnO NPs further underscore their potential for biomedical applications. The high isolation rate of MRSA strains worrying for the need for constant monitoring of their spreading and searching for alternative treatment strategies involving their prevention and control. Valuable research finding was the effective inhibitory activity of ZnO NPs synthesized via an ecofriendly method exhibited against MRSA and MSSA at low concentration. Also, these NPs can combat the antimicrobial resistant bacterial isolates through significant eradication of their pre-formed biofilm in biomedical settings. While this study highlights the promising potential of myco-synthesized ZnO NPs as a hopeful bioactive agent, several research gaps remain. Exploration of their efficacy against a broader spectrum of pathogens are needed to establish their versatility. Also, cytotoxicity testing utilizing a broader range of normal cell lines are required to further validate the selectivity of ZnO NPs toward cancer cells. Additionally, their long-term stability, biocompatibility, potential in vivo toxicity, and precise mechanisms underlying their bioactivities are yet to be fully elucidated.

Data availability

The datasets used and/or analysed during the current study available from the corresponding author on reasonable request.

Received: 12 February 2025; Accepted: 20 May 2025

Published online: 29 May 2025

References

- Salah, N. M., Saafan, A. E., Salem, E. H. & El Rabey, H. A. Inhibition of the Vancomycin resistance in *Staphylococcus aureus* in Egypt using silver nanoparticles. **2022**, 7380147. (2022). <https://doi.org/10.1155/2022/7380147>
- Hao, Y. et al. Advances in antibacterial activity of zinc oxide nanoparticles against *Staphylococcus aureus* (Review). *Biomed. Rep.* **21** (5), 161. <https://doi.org/10.3892/br.2024.1849> (2024).
- Dhungel, S. & Rijal, K. R. Methicillin-resistant *Staphylococcus aureus* (MRSA): prevalence, antimicrobial susceptibility pattern, and detection of *MecA* gene among cardiac patients from a tertiary care heart center in Kathmandu. *Nepal J.* **14**, 11786337211037355. <https://doi.org/10.1177/11786337211037355> (2021).
- Tong, S. Y. C., Davis, J. S., Eichenberger, E., Holland, T. L. & Fowler, V. G. *Staphylococcus aureus* infections: epidemiology, pathophysiology, clinical manifestations, and management. **28**(3), 603–661. <https://doi.org/10.1128/cmr.00134-14> (2015).
- Organization, W. H. *Global Antimicrobial Resistance and Use Surveillance System (GLASS) Report 2022* (World Health Organization, 2022).
- Abebe, A. A. & Birhanu, A. G. Methicillin resistant *Staphylococcus aureus*: molecular mechanisms underlying drug resistance development and novel strategies to combat. *Infect. Drug Resist.* **16**, 7641–7662. <https://doi.org/10.2147/idr.s428103> (2023).
- Jani, K., Mehta, S., Patel, R., Prajapati, B. & Patel, G. J. C. M. C. Focused insights into liposomal nanotherapeutics for antimicrobial treatment. (2024).
- Wu, X. et al. *Staphylococcus aureus* biofilm: formulation, regulatory, and emerging natural products-derived therapeutics. *Biofilm* **7**, 100175. <https://doi.org/10.1016/j.biofilm.2023.100175> (2024).
- Aniba, R. et al. Characterization of biofilm formation in uropathogenic *Staphylococcus aureus* and their association with antibiotic resistance. *Microbe* **2**, 100029. <https://doi.org/10.1016/j.microb.2023.100029> (2024).
- Aslam, B. et al. Antibiotic resistance: a rundown of a global crisis. *Infect. Drug Resist.* **11** (null), 1645–1658. <https://doi.org/10.2147/IDR.S173867> (2018).
- Liang, S. et al. Bacteriophage therapy as application bacterial infection in China **12**(2), 417 (2023).

12. Rasheed, R. & Bhat, A. Biogenic synthesis of selenium and copper oxide nanoparticles and inhibitory effect against multi-drug resistant biofilm-forming bacterial pathogens **12**(5). <https://doi.org/10.3390/biomedicines12050994> (2024).
13. Abd El-Hamid, M. I. et al. Tackling strong biofilm and multi-virulent vancomycin-resistant *Staphylococcus aureus* via natural alkaloid-based porous nanoparticles: perspective towards near future eradication. *Front. Cell. Infect. Microbiol.* **13**, 1287426. <https://doi.org/10.3389/fcimb.2023.1287426> (2023).
14. Rizwan, M. et al. Enterobacter hormaechei-driven novel biosynthesis of Tin oxide nanoparticles and evaluation of their anti-aging, cytotoxic, and enzyme inhibition potential. *ACS Omega*. **8** (30), 27439–27449 (2023).
15. Ly, P.-D. et al. Recent advances in surface decoration of nanoparticles in drug delivery. *Front. Nanotechnol.* **6**, 1456939 (2024).
16. Saqib, S. et al. Postharvest disease inhibition in fruit by synthesis and characterization of Chitosan iron oxide nanoparticles. *Biocatal. Agric. Biotechnol.* **28**, 101729. <https://doi.org/10.1016/j.bcab.2020.101729> (2020).
17. Saqib, S. et al. Bimetallic assembled silver nanoparticles impregnated in *Aspergillus fumigatus* extract damage the bacterial membrane surface and release cellular contents. *Coatings* **12** (10), 1505 (2022).
18. Faisal, S. et al. Biofabrication of silver nanoparticles employing biomolecules of paraclostridium benzoelyticum strain: its characterization and their in-vitro antibacterial, anti-aging, anti-cancer and other biomedical applications. *Microsc. Res. Technol.* **86** (7), 846–861 (2023).
19. Khan, Y. et al. Classification, synthetic, and characterization approaches to nanoparticles, and their applications in various fields of nanotechnology. *Review* **12** (11), 1386 (2022).
20. Boopalan, M., Revathi Ganesh, C. & Arumugam, S. Chapter 1 - Introduction to the carbon-based nanomaterials and its unique electrochemical and physicochemical properties. In: (eds Biswas, K., Mohanta, Y. K., Mohanta, T. K. & Saravanan, M.) Carbon-Based Nanomaterials in Biosystems. Academic; 3–29. (2024).
21. Ahire, S. A. et al. The augmentation of nanotechnology era: a concise review on fundamental concepts of nanotechnology and applications in material science and technology. *Results Chem.* **4**, 100633. <https://doi.org/10.1016/j.rechem.2022.100633> (2022).
22. Anucha, C. B. & Guénin, E. Micro and nanotechnology. In: (eds Gunduz, O., Egles, C., Pérez, R. A., Ficaí, D. & Ustundag, C. B.) Biomaterials and Tissue Engineering. Cham: Springer International Publishing; 131–174. (2023).
23. Saqib, S. et al. Organometallic assembling of chitosan-Iron oxide nanoparticles with their antifungal evaluation against rhizopus oryzae. *Appl. Organomet. Chem.* **33** (11), e5190. <https://doi.org/10.1002/aoc.5190> (2019).
24. Ali, A., Phull, A.-R. & Zia, M. Elemental zinc to zinc nanoparticles: is ZnO NPs crucial for life? Synthesis, toxicological, and environmental concerns. **7**(5), 413–441. <https://doi.org/10.1515/ntrev-2018-0067> (2018).
25. Gulab, H. et al. Advancements in zinc oxide nanomaterials: synthesis, properties, and diverse applications. *Nano Struct. Nano Obj.* **39**, 101271. <https://doi.org/10.1016/j.nanoso.2024.101271> (2024).
26. Patel, K. D. et al. Oxidative stress modulating nanomaterials and their biochemical roles in nanomedicine. **9**(10), 1630–1682 (2024).
27. Islam, F. et al. Exploring the journey of zinc oxide nanoparticles (ZnO-NPs). *Toward Biomed. Appl.* **15** (6), 2160 (2022).
28. Saqib, S. et al. Catalytic potential of endophytes facilitates synthesis of biometallic zinc oxide nanoparticles for agricultural application. *BioMetals* **35** (5), 967–985. <https://doi.org/10.1007/s10534-022-00417-1> (2022).
29. Mohd Yusof, H., Abdul Rahman, N. A., Mohamad, R., Hasanah Zaidan, U. & Samsudin, A. A. Antibacterial potential of biosynthesized zinc oxide nanoparticles against poultry-associated foodborne pathogens: an in vitro study. **11**(7), 2093 (2021).
30. Kirubakaran, D. et al. A comprehensive review on the green synthesis of nanoparticles: advancements in biomedical and environmental applications. *Biomed. Mater. Devices*. <https://doi.org/10.1007/s44174-025-00295-4> (2025).
31. Abid, N. et al. Synthesis of nanomaterials using various top-down and bottom-up approaches, influencing factors, advantages, and disadvantages: a review. *Adv. Colloid Interface Sci.* **300**, 102597. <https://doi.org/10.1016/j.cis.2021.102597> (2022).
32. Zain Ul Abidin, M. et al. A comprehensive review on the synthesis of ferrite nanomaterials via bottom-up and top-down approaches advantages, disadvantages, characterizations and computational insights. *Coord. Chem. Rev.* **520**, 216158. <https://doi.org/10.1016/j.ccr.2024.216158> (2024).
33. Srivastava, S. & Bhargava, A. Green nanotechnology: an overview. In: (eds Srivastava, S. & Bhargava, A.) Green Nanoparticles: the Future of Nanobiotechnology. Singapore: Springer Singapore; 1–13. (2022).
34. Mazari, S. A. et al. Nanomaterials: applications, waste-handling, environmental toxicities, and future challenges: a review. *J. Environ. Chem. Eng.* **9** (2), 105028. <https://doi.org/10.1016/j.jece.2021.105028> (2021).
35. Singh, H. & Kaur, K. Role of nanotechnology in research fields: medical sciences, military & tribology: a review on recent advancements, grand challenges and perspectives. *Mater. Today Proc.* <https://doi.org/10.1016/j.matpr.2023.02.061> (2023).
36. Zafar, S. et al. Development of Iron nanoparticles (FeNPs) using biomass of enterobacter: its characterization, antimicrobial, anti-Alzheimer's, and enzyme inhibition potential. *Micromachines* **13** (8), 1259 (2022).
37. Qamar, S. U. R., Ahmad, J. N. & Nanoparticles mechanism of biosynthesis using plant extracts, bacteria, fungi, and their applications. *J. Mol. Liq.* **334**, 116040. <https://doi.org/10.1016/j.molliq.2021.116040> (2021).
38. Jeevanandam, J. et al. Green approaches for the synthesis of metal and metal oxide nanoparticles using microbial and plant extracts. *Nanoscale* **14** (7), 2534–2571. <https://doi.org/10.1039/D1NR08144F> (2022).
39. Faisal, S. et al. Paraclostridium benzoelyticum Bacterium-Mediated zinc oxide nanoparticles and their in vivo multiple biological applications. *Oxidative Med. Cell. Longev.* **2022** (1), 5994033. <https://doi.org/10.1155/2022/5994033> (2022).
40. Faisal, S. et al. Bio-catalytic activity of novel *Mentha arvensis* intervened biocompatible magnesium oxide nanomaterials. *Catalysts* **11** (7), 780 (2021).
41. Abdullah, Al-Radadi, N. S., Hussain, T., Faisal, S. & Ali Raza Shah, S. Novel biosynthesis, characterization and bio-catalytic potential of green algae (*Spirogyra hyalina*) mediated silver nanomaterials. *Saudi J. Biol. Sci.* **29** (1), 411–419. <https://doi.org/10.1016/j.sjbs.2021.09.013> (2022).
42. Khan, M. I. et al. *Monotheca buxifolia* driven synthesis of zinc oxide nano material its characterization and biomedical applications. *Micromachines* **13** (5), 668 (2022).
43. Shah, S. et al. Engineering novel gold nanoparticles using *Sageretia thea* leaf extract and evaluation of their biological activities. *J. Nanostruct. Chem.* **12** (1), 129–140. <https://doi.org/10.1007/s40097-021-00407-8> (2022).
44. Abdullah, R., Au, Faisal, S., Almostafa, M. M., Younis, N. S. & Yahya, G. Multifunctional *Spirogyra-hyalina*-mediated barium oxide nanoparticles (BaONPs): synthesis and applications. *Molecules* **28** (17), 6364 (2023).
45. Saravanan, A. et al. A review on biosynthesis of metal nanoparticles and its environmental applications. *Chemosphere* **264**, 128580. <https://doi.org/10.1016/j.chemosphere.2020.128580> (2021).
46. Asghar, M. et al. Synthesis and characterization of microbial mediated cadmium oxide nanoparticles. *Microsc. Res. Technol.* **83** (12), 1574–1584. <https://doi.org/10.1002/jemt.23553> (2020).
47. Hashem, A. H., Al-Askar, A. A., Haponiuk, J., Abd-Elsalam, K. A. & Hasanin, M. S. Biosynthesis, characterization, and antifungal activity of novel trimetallic copper oxide–Selenium–Zinc oxide nanoparticles against some Mucorales fungi. *Microorganisms*. **11**(6), 1380 (2023).
48. Meera, C. R., Zaynitdinova, L. & Great, U. Sustainable production of nanoparticles from Fungi and their agricultural applications. In: (eds Mohanta, Y. K., Mishra, B. & Pudake, R. N.) Nano-microbiology for Sustainable Development. Cham: Springer Nature Switzerland; 71–103. (2025).
49. Sidhu, A. K., Verma, N. & Kaushal, P. Role of biogenic capping agents in the synthesis of metallic nanoparticles and evaluation of their therapeutic potential. *Front. Nanotechnol.* **3**. <https://doi.org/10.3389/fnano.2021.801620> (2022).

50. Ahmed, S. F. et al. Green approaches in synthesising nanomaterials for environmental nanobioremediation: technological advancements, applications, benefits and challenges. *Environ. Res.* **204**, 111967. <https://doi.org/10.1016/j.envres.2021.111967> (2022).
51. Espinosa-Ortiz, E. J., Rene, E. R. & Gerlach, R. Potential use of fungal-bacterial co-cultures for the removal of organic pollutants. *Crit. Rev. Biotechnol.* **42** (3), 361–383. <https://doi.org/10.1080/07388551.2021.1940831> (2022).
52. Al-Radadi, N. S. et al. Zingiber officinale driven bioproduction of ZnO nanoparticles and their anti-inflammatory, anti-diabetic, anti-Alzheimer, anti-oxidant, and anti-microbial applications. *Inorg. Chem. Commun.* **140**, 109274. <https://doi.org/10.1016/j.inoche.2022.109274> (2022).
53. Jan, H. et al. Plant-based synthesis of zinc oxide nanoparticles (ZnO-NPs) using aqueous leaf extract of *Aquilegia pubiflora*: their antiproliferative activity against HepG2 cells inducing reactive oxygen species and other in vitro properties. *Oxidative Med. Cell. Longev.* **2021** (1), 4786227. <https://doi.org/10.1155/2021/4786227> (2021).
54. Faisal, S. et al. Green synthesis of zinc oxide (ZnO) nanoparticles using aqueous fruit extracts of *myristica fragrans*: their characterizations and biological and environmental applications. *ACS Omega*. **6** (14), 9709–9722 (2021).
55. Rehman, H. et al. Delphinium uncinatum mediated biosynthesis of zinc oxide nanoparticles and in-vitro evaluation of their antioxidant, cytotoxic, antimicrobial, anti-diabetic, anti-inflammatory, and anti-aging activities. *Saudi J. Biol. Sci.* **30** (1), 103485. <https://doi.org/10.1016/j.sjbs.2022.103485> (2023).
56. Anjum, S. et al. Recent advances in zinc oxide nanoparticles (ZnO NPs) for cancer diagnosis. *Target. Drug Deliv. Treat.* **13** (18), 4570 (2021).
57. Okaiyeto, K., Gigliobianco, M. R. & Di Martino, P. Biogenic zinc oxide nanoparticles as a promising antibacterial agent: synthesis and characterization. *Int. J. Mol. Sci.* **25** (17), 9500 (2024).
58. Procop, G. W., Church, D. L., Hall, G. S. & Janda, W. M. *Koneman's color atlas and textbook of diagnostic microbiology* (Jones & Bartlett Learning, 2020).
59. Ibrahim, D. D. et al. An emerging zoonosis: molecular detection of multidrug-methicillin resistant *Staphylococcus aureus* from butchers' knives, livestock products and contact surfaces. *Vet. Res. Commun.* **48** (3), 1697–1705. <https://doi.org/10.1007/s11259-024-10346-8> (2024).
60. Rostami, S., Moosavian, M., Shoja, S., Torabipour, M. & Farshadzadeh, Z. Comparison of Meca gene-based PCR with CLSI cefoxitin and Oxacillin disc diffusion methods for detecting methicillin resistance in *Staphylococcus aureus* clinical isolates. *Afr. J. Microbiol. Res.* **7** (21), 2438–2441 (2013).
61. Elkady, F. M. et al. Comparative genotypic analysis of RAPD and RFLP markers for molecular variation detection of methicillin-resistant *Staphylococcus aureus* clinical isolates. **58**(9). <https://doi.org/10.3390/medicina58091245> (2022).
62. Hashem, A. H., Abu-Elreesh, G., El-Sheikh, H. H. & Suleiman, W. B. Isolation, identification, and statistical optimization of a psychrotolerant *Mucor racemosus* for sustainable lipid production. *Biomass Convers. Biorefin.* **13** (4), 3415–3426. <https://doi.org/10.1007/s13399-022-02390-8> (2023).
63. Mohamed Aly Khalil, A. & Hosny Hashem, A. Morphological changes of conidiogenesis in two *Aspergillus* species. *J. Pure Appl. Microbiol.* **12** (4), 2041–2048 (2018).
64. Hashem, A. H., Hasanin, M. S., Khalil, A. M. A. & Suleiman, W. B. Eco-Green conversion of watermelon peels to single cell oils using a unique oleaginous fungus: *lichtheimia corymbifera* AH13. *Waste Biomass Valoriz.* **11** (11), 5721–5732. <https://doi.org/10.1007/s12649-019-00850-3> (2020).
65. Omran, B. A. & Baek, K-H. Dual extracellular mycofabrication of Cobalt and zinc nano metal oxides mediated by mycelial-cell free filtrate of *Aspergillus Sojae*: characterization and assessment of antibacterial activity. *J. Mol. Struct.* **1300**, 137190. <https://doi.org/10.1016/j.molstruc.2023.137190> (2024).
66. Venu Gopal, V. R. & Kamila, S. Effect of temperature on the morphology of ZnO nanoparticles: a comparative study. *Appl. Nanosci.* **7** (3), 75–82. <https://doi.org/10.1007/s13204-017-0553-3> (2017).
67. Khalil, A., Abdelaziz, A., Khaleil, M. & Hashem, A. Fungal endophytes from leaves of *Avicennia marina* growing in semi-arid environment as a promising source for bioactive compounds. *Lett. Appl. Microbiol.* **72** (3), 263–274 (2021).
68. Van de Loosdrecht, A., Beelen, R., Ossenkoppele g. Broekhoven, M. & Langenhuijsen, M. A tetrazolium-based colorimetric MTT assay to quantitate human monocyte mediated cytotoxicity against leukemic cells from cell lines and patients with acute myeloid leukemia. *J. Immunol. Methods.* **174** (1–2), 311–320 (1994).
69. Hashem, A. H. et al. Pomegranate Peel extract stabilized selenium nanoparticles synthesis: promising antimicrobial potential, antioxidant activity, biocompatibility, and hemocompatibility. **195**(10), 5753–5776. <https://doi.org/10.1007/s12010-023-04326-y> (2023).
70. Elkady, F. M. et al. Unveiling the *Launaea nudicaulis* (L.) Hook medicinal bioactivities: phytochemical analysis, antibacterial, antibiofilm, and anticancer activities. *Front. Microbiol.* **15**, 1454623. <https://doi.org/10.3389/fmicb.2024.1454623> (2024).
71. Arsene, M. M. J. et al. Synthesis of green-engineered silver nanoparticles using *Cymbopogon citratus* (lemongrass) and its antibacterial activity against clinical *Pseudomonas aeruginosa*. *Int. J. One Health* 100–113 (2024).
72. Elkady, F. M. et al. Genetic insights on meropenem resistance concerning *Klebsiella pneumoniae* clinical isolates. *Life* **14** (11), 1408 (2024).
73. Chen, Q. et al. Bactericidal and biofilm eradication efficacy of a fluorinated benzimidazole derivative, TFBZ, against methicillin-resistant *Staphylococcus aureus*. *Front. Pharmacol.* **15**, 1342821. <https://doi.org/10.3389/fphar.2024.1342821> (2024).
74. Shahzad, M. A. et al. Virulence and resistance profiling of *Staphylococcus aureus* isolated from subclinical bovine mastitis in the Pakistani Pothohar region. *Sci. Rep.* **14** (1), 14569. <https://doi.org/10.1038/s41598-024-65448-9> (2024).
75. Minhas, B. et al. Identification, antimicrobial resistance profiling and virulence factors of bacterial isolates recovered from human clinical cases. *J. Pure Appl. Microbiol.* **18**(4), 2850–2861. <https://doi.org/10.22207/JPAM.18.4.56> (2024).
76. Maharjan, S. & Ansari, M. Phenotypic detection of methicillin resistance, biofilm production, and inducible clindamycin resistance in *Staphylococcus aureus* clinical isolates in Kathmandu, Nepal. *Trop. Med. Int. Health* **50**(1), 71. <https://doi.org/10.1186/s41182-022-00460-1> (2022).
77. Tawfeek, C. E., Khattab, S., Elmaraghy, N., Heiba, A. A. & Nageeb, W. M. Reduced Vancomycin susceptibility in *Staphylococcus aureus* clinical isolates: a spectrum of less investigated uncertainties. *BMC Infect. Dis.* **24** (1), 1218. <https://doi.org/10.1186/s12879-024-10047-2> (2024).
78. Wang, W. Y., Chiu, C. F., Tsao, S. M., Lee, Y. L. & Chen, Y. H. Accurate prediction of antimicrobial resistance and genetic marker of *Staphylococcus aureus* clinical isolates using MALDI-TOF MS and machine learning—across DRIAMS and Taiwan database. *Int. J. Antimicrob. Agents.* **64** (5), 107329. <https://doi.org/10.1016/j.ijantimicag.2024.107329> (2024).
79. Zeghoud, S. et al. A review on biogenic green synthesis of ZnO nanoparticles by plant biomass and their applications. *Mater. Today Commun.* **33**, 104747. <https://doi.org/10.1016/j.mtcomm.2022.104747> (2022).
80. Singh, T. A. et al. A state of the Art review on the synthesis, antibacterial, antioxidant, antidiabetic and tissue regeneration activities of zinc oxide nanoparticles. *Adv. Colloid Interface Sci.* **295**, 102495. <https://doi.org/10.1016/j.cis.2021.102495> (2021).
81. Deb, D. & Sutradhar, A. Microalgal nanobiotechnology for biosynthesis of metallic nanoparticles: In-depth into the strategies, mechanism and nanofluidic hydrodynamics. *Biocatal. Agric. Biotechnol.* **56**, 103046. <https://doi.org/10.1016/j.bcab.2024.103046> (2024).
82. Kalpana, V. N. et al. Biosynthesis of zinc oxide nanoparticles using culture filtrates of *Aspergillus Niger*: antimicrobial textiles and dye degradation studies. *OpenNano* **3**, 48–55. <https://doi.org/10.1016/j.onano.2018.06.001> (2018).

83. Abdelhakim, H. K., El-Sayed, E. R. & Rashidi, F. B. Biosynthesis of zinc oxide nanoparticles with antimicrobial, anticancer, antioxidant and photocatalytic activities by the endophytic *Alternaria tenuissima*. *J. Appl. Microbiol.* **128**(6), 1634–46. <https://doi.org/10.1111/jam.14581J> (2020).
84. Sharma, J. L., Dhayal, V. & Sharma, R. K. White-rot fungus mediated green synthesis of zinc oxide nanoparticles and their impregnation on cellulose to develop environmental friendly antimicrobial fibers. *3 Biotech.* **11** (6), 269. <https://doi.org/10.1007/s13205-021-02840-6> (2021).
85. Abdelkader, D. H. et al. Zinc oxide nanoparticles as potential delivery carrier: green synthesis by *Aspergillus Niger* endophytic fungus, characterization, and in vitro/in vivo antibacterial activity. **15** (9), 1057 (2022).
86. Mohd Yusof, H., Abdul Rahman, N. A., Mohamad, R., Zaidan, U. H. & Samsudin, A. A. Biosynthesis of zinc oxide nanoparticles by cell-biomass and supernatant of *Lactobacillus plantarum* TA4 and its antibacterial and biocompatibility properties. *Sci. Rep.* **10** (1), 19996. <https://doi.org/10.1038/s41598-020-76402-w> (2020).
87. Ngom, I., Ngom, B. D., Sackey, J. & Khamlich, S. Biosynthesis of zinc oxide nanoparticles using extracts of *Moringa oleifera*: structural & optical properties. *Mater. Today Proc.* **36**, 526–533. <https://doi.org/10.1016/j.matpr.2020.05.323> (2021).
88. Umar, H., Kavaz, D. & Rizaner, N. Biosynthesis of zinc oxide nanoparticles using *Albizia lebeck* stem bark, and evaluation of its antimicrobial, antioxidant, and cytotoxic activities on human breast cancer cell lines. *Int. J. Nanomed.* **14** (null), 87–100. <https://doi.org/10.2147/IJN.S186888> (2019).
89. Al-Askar, A. A., Hashem, A. H., Elhussieny, N. I. & Saied, E. Green biosynthesis of zinc oxide nanoparticles using *Pluchea indica* leaf extract. *Antimicrob. Photocatal. Act.* **28** (12), 4679 (2023).
90. Salih, A. M. et al. Biosynthesis of zinc oxide nanoparticles using *Phoenix dactylifera* and their effect on biomass and phytochemical compounds in *Juniperus procera*. *Sci. Rep.* **11** (1), 19136. <https://doi.org/10.1038/s41598-021-98607-3> (2021).
91. Fouada, A. et al. Green synthesis of zinc oxide nanoparticles using an aqueous extract of *Punica granatum* for antimicrobial and catalytic activity. *J. Funct. Biomater.* **14**(4), 205 (2023).
92. Gao, Y. et al. Biofabrication of zinc oxide nanoparticles from *Aspergillus Niger*, their antioxidant, antimicrobial and anticancer activity. *J. Clust. Sci.* **30** (4), 937–946. <https://doi.org/10.1007/s10876-019-01551-6> (2019).
93. Natrayan, L. et al. Eco-friendly zinc oxide nanoparticles from *Moringa oleifera* leaf extract for photocatalytic and antibacterial applications. *Clean Technol. Environ. Policy.* <https://doi.org/10.1007/s10098-024-02814-1> (2024).
94. Chinnasamy, G., Chandrasekharan, S., Koh, T. W., & Bhatnagar, S. Synthesis characterization, antibacterial and wound healing efficacy of silver nanoparticles from *Azadirachta indica*. **12**. <https://doi.org/10.3389/fmicb.2021.611560> (2021).
95. Rane, A. N., Baikar, V. V., Ravi Kumar, V. & Deopurkar, R. L. Agro-Industrial wastes for production of biosurfactant by *Bacillus subtilis* ANR 88 and its application in synthesis of silver and gold nanoparticles. **8**. <https://doi.org/10.3389/fmicb.2017.00492> (2017).
96. Punitha, U. & Mary Saral, A. Nickel oxide nanoparticles from *sargassumwightii*: synthesis, characterization, and biomedical applications. *Results Chem.* **7**, 101289. <https://doi.org/10.1016/j.rechem.2023.101289> (2024).
97. Shrestha, S., Wang, B. & Dutta, P. Nanoparticle processing: understanding and controlling aggregation. *Adv. Colloid Interface Sci.* **279**, 102162. <https://doi.org/10.1016/j.cis.2020.102162> (2020).
98. Moeni, M. et al. Effect of reaction and post-treatment conditions on physico-chemical properties of magnetic iron oxide nanoparticles. *Particuology* **91**, 155–167. <https://doi.org/10.1016/j.partic.2024.02.006> (2024).
99. Chong, W. J. et al. Biodegradable PLA-ZnO nanocomposite biomaterials with antibacterial properties, tissue engineering viability, and enhanced biocompatibility. *Smart Mater. Manuf.* **1**, 100004. <https://doi.org/10.1016/j.smmf.2022.100004> (2023).
100. Stielow, M. et al. The bioavailability of drugs—the current state of knowledge **28** (24), 8038 (2023).
101. Österberg, M., Henn, K. A., Farooq, M. & Valle-Delgado, J. J. Biobased nanomaterials: the role of interfacial interactions for advanced materials. *Chem. Rev.* **123** (5), 2200–2241. <https://doi.org/10.1021/acs.chemrev.2c00492> (2023).
102. Midekessa, G. et al. Zeta potential of extracellular vesicles: toward understanding the attributes that determine colloidal stability. *ACS Omega*. **5** (27), 16701–16710. <https://doi.org/10.1021/acsomega.0c01582> (2020).
103. Pochapski, D. J., Carvalho dos Santos, C., Leite, G. W., Pulcinelli, S. H. & Santilli, C. V. Zeta potential and colloidal stability predictions for inorganic nanoparticle dispersions: effects of experimental conditions and electrokinetic models on the interpretation of results. *Langmuir* **37** (45), 13379–13389. <https://doi.org/10.1021/acs.langmuir.1c02056> (2021).
104. Verma, R., Pathak, S., Srivastava, A. K., Prawer, S. & Tomljenovic-Hanic, S. ZnO nanomaterials: green synthesis, toxicity evaluation and new insights in biomedical applications. *J. Alloys Compd.* **876**, 160175. <https://doi.org/10.1016/j.jallcom.2021.160175> (2021).
105. Caramella, C. J. B. Nanotheranostics. Inorganic drug release from mesoporous silica nanoparticles for Cancer treatment. *Biosens. Nanotheranostics* **2**(1), 1–6 (2023).
106. Priyadarshini, E., Priyadarshini, S. S., Cousins, B. G. & Pradhan, N. Metal-fungus interaction: review on cellular processes underlying heavy metal detoxification and synthesis of metal nanoparticles. *Chemosphere* **274**, 129976. <https://doi.org/10.1016/j.chemosphere.2021.129976> (2021).
107. Kuhar, N., Sil, S. & Umapathy, S. Potential of Raman spectroscopic techniques to study proteins. *Spectrochim. Acta Part A Mol. Biomol. Spectrosc.* **258**, 119712. <https://doi.org/10.1016/j.saa.2021.119712> (2021).
108. Batool, M., Saba, M. & Albsher, G. J. A. P. Wild Mushroom (*Ganoderma multipileum*) as Biosource for Zinc oxide Nanoparticles: From Synthesis to Enhance Biological Applications. (2023).
109. Dey, S. et al. A critical review on zinc oxide nanoparticles: synthesis, properties and biomedical applications. *Intell. Pharm.* <https://doi.org/10.1016/j.ipha.2024.08.004> (2024).
110. Hammad, S. E., El-Rouby, M. N., Abdel-Aziz, M. M., El-Sayyad, G. S. & Elshikh, H. H. Endophytic fungi-assisted biomass synthesis of gold, and zinc oxide nanoparticles for increasing antibacterial, and anticancer activities. *Biomass Convers. Biorefin.* **15** (2), 2285–2302. <https://doi.org/10.1007/s13399-023-04954-8> (2025).
111. Majeed, S., Danish, M. & Norazmi, F. S. B. Fungal derived zinc oxide nanoparticles and their antibacterial and anticancer activities against human alveoli lung cancer A-549 cell line. *Adv. Sci. Eng. Med.* **10** (6), 551–556 (2018).
112. Anjum, S., Hashim, M., Malik, S. A., Khan, M. & Lorenzo, J. M. Recent advances in zinc oxide nanoparticles (ZnO NPs) for Cancer diagnosis. *Target. Drug Deliv. Treat.* **13** (18). <https://doi.org/10.3390/cancers13184570> (2021).
113. Gu, W. & Yang, C. Zinc oxide nanoparticles inhibit malignant progression and chemotherapy resistance of ovarian cancer cells by activating endoplasmic reticulum stress and promoting autophagy. *Exp. Ther. Med.* **26** (5), 508. <https://doi.org/10.3892/etm.2023.12207> (2023).
114. Khalil, I. & Yehye, W. A. Nanoantioxidants: recent trends in antioxidant delivery applications. *Antioxidants* **9**(1). <https://doi.org/10.3390/antiox9010024> (2019).
115. Manzoor, M. A. et al. Nanotechnology-based approaches for promoting horticulture crop growth, antioxidant response and abiotic stresses tolerance. *Plant. Stress.* **11**, 100337. <https://doi.org/10.1016/j.stress.2023.100337> (2024).
116. Dai, Y. et al. Reactive oxygen species-scavenging nanomaterials for the prevention and treatment of age-related diseases. *J. Nanobiotechnol.* **22** (1), 252. <https://doi.org/10.1186/s12951-024-02501-9> (2024).
117. Wang, Z. et al. Synthesis of zinc oxide nanoparticles and their applications in enhancing plant stress resistance: a review. *Agronomy* **13** (12), 3060 (2023).
118. Ng, C. T. et al. Zinc oxide nanoparticles exhibit cytotoxicity and genotoxicity through oxidative stress responses in human lung fibroblasts and *Drosophila melanogaster*. *Int. J. Nanomed.* **12**, 1621–1637. <https://doi.org/10.2147/ijn.s124403> (2017).

119. Murali, M., Kalegowda, N., Gowtham, H. G. & Ansari, M. A. Plant-mediated zinc oxide nanoparticles: advances in the new millennium towards understanding their therapeutic role in biomedical applications. *Pharmaceutics* **13**(10). <https://doi.org/10.3390/pharmaceutics13101662> (2021).
120. Agrawal, A., Sharma, A., Awasthi, G., Awasthi, A. & Awasthi, K. K. Toxicity Assessment and Antibacterial Activity of ZnO Nanoparticles, Nanostructured Zinc Oxide. 511–552 (Elsevier, 2021).
121. Abo-Shama, U. H. et al. Synergistic and antagonistic effects of metal nanoparticles in combination with antibiotics against some reference strains of pathogenic microorganisms. **13**, 351–362. <https://doi.org/10.2147/idr.s234425> (2020).
122. Cherian, T. et al. Myristica fragrans bio-active ester functionalized ZnO nanoparticles exhibit antibacterial and antibiofilm activities in clinical isolates. *J. Microbiol. Methods*. **166**, 105716. <https://doi.org/10.1016/j.mimet.2019.105716> (2019).
123. Ansari, M. A., Khan, H. M., Khan, A. A., Sultan, A. & Azam, A. Characterization of clinical strains of MSSA, MRSA and MRSE isolated from skin and soft tissue infections and the antibacterial activity of ZnO nanoparticles. *World J. Microbiol. Biotechnol.* **28** (4), 1605–1613. <https://doi.org/10.1007/s11274-011-0966-1> (2012).
124. Ibne Shoukani, H. et al. Ciprofloxacin loaded PEG coated ZnO nanoparticles with enhanced antibacterial and wound healing effects. *Sci. Rep.* **14** (1), 4689. <https://doi.org/10.1038/s41598-024-55306-z> (2024).
125. Mishra, P. K., Mishra, H., Ekielski, A., Talegaonkar, S. & Vaidya, B. Zinc oxide nanoparticles: a promising nanomaterial for biomedical applications. *Drug Discov. Today*. **22** (12), 1825–1834. <https://doi.org/10.1016/j.drudis.2017.08.006> (2017).
126. Rezić, I., Majdak, M. & Ljoljić Bilić, V. Development of antibacterial protective coatings active against MSSA and MRSA on biodegradable polymers. *Polymers* **13**(4). <https://doi.org/10.3390/polym13040659> (2021).
127. Riahi, S. et al. Bactericidal activity of ZnO nanoparticles against multidrug-resistant bacteria. *J. Mol. Liq.* **387**, 122596. <https://doi.org/10.1016/j.molliq.2023.122596> (2023).
128. Abdelraheem, W. M., Khairy, R. M. M., Zaki, A. I. & Zaki, S. H. Effect of ZnO nanoparticles on methicillin, Vancomycin, linezolid resistance and biofilm formation in *Staphylococcus aureus* isolates. *Ann. Clin. Microbiol. Antimicrob.* **20** (1), 54. <https://doi.org/10.1186/s12941-021-00459-2> (2021).
129. Khan, I. et al. Antibacterial efficacy of linezolid alone and in combination with zinc oxide nanoparticles against methicillin-resistant *S. Aureus* clinical isolates. *Biomedicine* **12** (3), 454–458 (2022).
130. Ahmed, N. A. & Othman, A. S. Green fabrication of ZnO nanoparticles via spirulina platensis and its efficiency against biofilm forming pathogens. *Microb. Cell. Fact.* **23** (1), 92 (2024).
131. Divya, M., Chen, J., Durán-Lara, E. F., Kim, K. & Vijayakumar, S. Revolutionizing healthcare: Harnessing nano biotechnology with zinc oxide nanoparticles to combat biofilm and bacterial infections—a short review. *Microb. Pathog.* **191**, 106679. <https://doi.org/10.1016/j.micpath.2024.106679> (2024).
132. Prakashkumar, N. et al. Comparative study of zinc oxide nanoparticles synthesized through biogenic and chemical route with reference to antibacterial, antibiofilm and anticancer activities. *Environ. Res.* **220**, 115136. <https://doi.org/10.1016/j.envres.2022.115136> (2023).
133. Kemung, H. M. et al. An optimized anti-adherence and anti-biofilm assay: case study of zinc oxide nanoparticles versus MRSA biofilm. *Progr. Microbes Mol. Biol.* **3**(1), 1–6. <https://doi.org/10.36877/pmmmb.a0000091> (2020).
134. Lahiri, D. et al. Anti-biofilm efficacy of green-synthesized ZnO nanoparticles on oral biofilm: in vitro and in silico study. *Front. Microbiol.* **13**, 939390 (2022).
135. Tian, X. et al. Zinc imidazole framework-8 nanoparticles disperse MRSA biofilm by inhibiting arginine biosynthesis and down-regulating adhesion-related proteins. *Adv. Mater. Interfaces*, **11**(14), 2300957 (2024).

Acknowledgements

All authors extend all respect to Zarqa University-Jordan for partial funding of this research.

Author contributions

Conceptualization: Ebrahim Saied & Amr H. Hashem; Methodology: Fathy M. Elkady, Bahaa M. Badr, Ebrahim Saied, Amr H. Hashem, Mohammed S. Abdulrahman, Mohammad M. Alkherkhis, Fahad M. Alshabrm, Eid A. Alatawi, Faris F. Aba Alkhayl, Ayman Salama; Data analysis, interpretation of results: Moselhy S. Mansy, Mohamed Aufy, Moselhy S. Mansy; Writing first draft and revision final manuscript: All Authors; Corresponding authors, responsible for communication with the journal: Amr H. Hashem & Mohamed Aufy.

Declarations

Competing interests

The authors declare no competing interests.

Ethics approval and consent to participate

Not applicable.

Consent for publication

Not applicable.

Additional information

Correspondence and requests for materials should be addressed to A.H.H. or M.A.

Reprints and permissions information is available at www.nature.com/reprints.

Publisher's note Springer Nature remains neutral with regard to jurisdictional claims in published maps and institutional affiliations.

Open Access This article is licensed under a Creative Commons Attribution-NonCommercial-NoDerivatives 4.0 International License, which permits any non-commercial use, sharing, distribution and reproduction in any medium or format, as long as you give appropriate credit to the original author(s) and the source, provide a link to the Creative Commons licence, and indicate if you modified the licensed material. You do not have permission under this licence to share adapted material derived from this article or parts of it. The images or other third party material in this article are included in the article's Creative Commons licence, unless indicated otherwise in a credit line to the material. If material is not included in the article's Creative Commons licence and your intended use is not permitted by statutory regulation or exceeds the permitted use, you will need to obtain permission directly from the copyright holder. To view a copy of this licence, visit <http://creativecommons.org/licenses/by-nc-nd/4.0/>.

© The Author(s) 2025